JEM Journal of Experimental Medicine

BRIEF DEFINITIVE REPORT

Distinct inflammatory Th17 subsets emerge in autoimmunity and infection

Ronald J. Bouch[1,4], Jing Zhang[1], Brandi C. Miller[1,4], Caroline J. Robbins[1], Timothy H. Mosher[1,4], Wencheng Li[2], Sergey A. Krupenko[5], Ravinder Nagpal[6], Jun Zhao[7], Richard S. Bloomfeld[8], Yong Lu[9], Mikhail A. Nikiforov[10], Qianqian Song[3], and Zhiheng He[1,3,11]

Th17 cells play a critical role in both tissue homeostasis and inflammation during clearance of infections as well as autoimmune and inflammatory disorders. Despite numerous efforts to distinguish the homeostatic and inflammatory roles of Th17 cells, the mechanism underlying the divergent functions of inflammatory Th17 cells remains poorly understood. In this study, we demonstrate that the inflammatory Th17 cells involved in autoimmune colitis and those activated during colitogenic infection are distinguishable populations characterized by their differential responses to the pharmacological molecule, clofazimine (CLF). Unlike existing Th17 inhibitors, CLF selectively inhibits proautoimmune Th17 cells while preserving the functional state of infection-elicited Th17 cells partially by reducing the enzyme ALDH1L2. Overall, our study identifies two distinct subsets within the inflammatory Th17 compartment with distinct regulatory mechanisms. Furthermore, we highlight the feasibility to develop disease-promoting Th17 selective inhibitor for treating autoimmune diseases.

Introduction

IL-17–producing T helper (Th17) cells, whose differentiation is governed by the transcription factor RORγt (Ivanov et al., 2006), are major contributors to inflammation (inflammatory Th17) during infection clearance (Collins et al., 2014; Kullberg et al., 2006; Omenetti et al., 2019) as well as autoimmune and inflammatory disorders (Hue et al., 2006; Lee et al., 2020). The primary pathway used to characterize and target inflammatory Th17 cells is through IL-23 signaling (Awasthi et al., 2009; McGeachy et al., 2009; Yen et al., 2006). Depletion or ablation of IL-23 in mice results in suppression of autoimmunity but vulnerability to pathogen infections (Kullberg et al., 2006; Ru et al., 2021; Withers et al., 2016). While Th17 cells secrete primarily IL-17A under homeostatic conditions, after being exposed to IL-23 during autoimmune responses or infection, they undergo transcriptional reprogramming to adopt a Th1-like profile, producing IFN-γ, referred to as Th1-like Th17 (Hirota et al., 2011). The production of IFN-γ is required for both the development of autoimmune and chronic inflammatory diseases (e.g., multiple sclerosis and inflammatory bowel diseases [IBD]; Powrie et al., 1994) and clearance of infections such as *Citrobacter rodentium* (Shiomi et al., 2010).

The importance of IL23–IFN-γ axis suggests that proautoimmune and anti-infection potential of Th17 are dependent on similar underlying mechanisms, including the utilization of aerobic glycolysis to provide energy and metabolites (Omenetti et al., 2019; Wu et al., 2020). However, recent studies reported that molecules identified to restrain (e.g., CD5L; Wagner et al., 2021) or promote (e.g., Gpr65; Gaublomme et al., 2015) Th17 pathology in autoimmunity have no conserved functions in infection-elicited Th17 cells (Omenetti et al., 2019), leading to an open question whether anti-infection and proautoimmunity functions of Th17 cells are conducted by subsets with distinguishable transcriptional and metabolic programs.

Generating inflammatory Th17 cells with distinct functions is challenging due to the lack of methods that recapitulate niche tissue conditions during pathogen infection or autoimmunity.

[1]Department of Microbiology and Immunology, Wake Forest School of Medicine, Winston-Salem, NC, USA; [2]Department of Pathology, Wake Forest School of Medicine, Winston-Salem, NC, USA; [3]Comprehensive Cancer Center, Wake Forest School of Medicine, Winston-Salem, NC, USA; [4]Department of Biology, Wake Forest University, Winston-Salem, NC, USA; [5]Department of Nutrition, Nutrition Research Institute, University of North Carolina, Kannapolis, NC, USA; [6]Department of Nutrition and Integrative Physiology, Florida State University, Tallahassee, FL, USA; [7]Florida Research and Innovation Center, Cleveland Clinic, Port St. Lucie, FL, USA; [8]Department of Gastroenterology, Wake Forest School of Medicine, Winston-Salem, NC, USA; [9]The Methodist Hospital Research Institute, Houston, TX, USA; [10]Department of Pathology, Duke University, Durham, NC, USA; [11]Department of Molecular Microbiology and Immunology, Keck School of Medicine, University of Southern California, Los Angeles, CA, USA.

Correspondence to Zhiheng He: zhihengh@usc.edu; Qianqian Song: qsong@wakehealth.edu; Mikhail A. Nikiforov: mikhail.nikiforov@duke.edu; Yong Lu: ylu2@houstonmethodist.org

Z. He is the lead contact.

Th17 cells primed in vitro with IL-6, IL-1β, and IL-23 mimic proautoimmune Th17 cells as they provoke autoimmune disease following transfer into mice (Ghoreschi et al., 2010; Langrish et al., 2005). However, it is unclear, to which extent these cells reflect the features of anti-infection Th17 cells. Alternatively, inflammatory Th17 cells can be isolated from autoimmune and infection murine models, but the dynamic reprogramming of Th17 cells complicates interpretations of differences amongst populations.

To address this challenge, we treated in vivo–committed Th17 cells present during either autoimmunity or infection with a panel of FDA-approved drugs. We hypothesized that Th17 cells from inflamed tissues would have comparable responses to pharmacological molecules if they were regulated similarly. However, we discovered that Th17 cells engaged in autoimmune colitis and those involved in the *C. rodentium* infection–induced colitis have distinct responses to a pharmacological molecule, clofazimine (CLF), indicating that they are two distinguishable populations. CLF selectively inhibits proautoimmune Th17 cells while preserving the functional state of infection-elicited Th17 cells partially through reducing mitochondrial enzyme ALDH1L2 (Krupenko et al., 2010) and subsequently elevating intracellular serine. Mechanistically, increased serine alters global epigenetic modifications from proautoimmune Th17 cells, resulting in the repression of proinflammatory cytokines. Our findings suggest that there are two functionally distinct inflammatory Th17 populations that are experimentally and therapeutically distinguishable.

Results and discussion

Inflammatory Th17 cells elicited by bacterial infection or autoimmunity are distinguishable

To investigate inherent differences between inflammatory Th17 cells engaged in autoimmunity versus those involved in anti-infection immunity, we isolated T cells from draining lymph nodes of murine models with autoimmune diseases, including experimental autoimmune encephalomyelitis (EAE) and T cell transfer–induced colitis, and compared them with those from *C. rodentium* infection. We compared the cytokine production of committed Th17 cells to a panel of FDA-approved pharmacological small molecules (Fig. 1 A). Th17 cells from all three models expressed IFN-γ, indicating their potential for inflammation, which is consistent with previously published reports on Th17 cells involved in autoimmunity and infection. While desonide, a steroid immune suppressor, non-selectively repressed the expression of IFN-γ from Th17 compartment, one molecule called CLF selectively reduced the IFN-γ production from autoimmune-associated but not *C. rodentium*–elicited Th17 cells (Fig. 1 B and Fig. S1, A–C). This suggests that there are distinctions between inflammatory Th17 cells from autoimmune and infection models and the possibility of selectively targeting proautoimmune Th17 cells while sparing anti-infection counterparts.

To further investigate the effects of CLF on Th17-dependent autoimmunity and bacterial clearance, we conducted in vivo experiments. While CLF did protect mice from the progression of EAE (Fig. S1 D), we chose to compare T cell transfer–induced autoimmune colitis, a murine model which replicates the key features of human IBD in experimental settings, with *C. rodentium* infection–induced colitis (Eden, 2019) for fairness of comparison. Consistent with ex vivo treatment, mice receiving a human-equivalent dosage of CLF (Nair and Jacob, 2016) had attenuated transfer colitis, as characterized by rescued body weight loss (Fig. 1 C), reduced colonic edema (Fig. S1, E and F), and lower clinical scores of colonic histopathology (Fig. 1 D). The attenuation in inflammation was restricted to transfer colitis model, as CLF-treated mice had no deficiencies in clearing bacterial burden or in colon pathology (Fig. 1, E and F). Although CLF is an FDA-approved drug against *Mycobacterium leprae* (Arbiser and Moschella, 1995; Yew et al., 2017), we observed no antibacterial activity against *C. rodentium* in vitro or during infection (Fig. S1, G and H).

To investigate Th17 responses to CLF in vivo, we next characterized the cytokine production of Th17 cells ($CD45^+CD3^+CD4^+ROR\gamma t^+$) recovered from inflamed colons. We observed a slight reduction in the total number of colonic Th17 cells between CLF- and vehicle-treated mice in the autoimmune colitis model (Fig. S1 I). However, CLF significantly reduced the frequency and amount of IFN-γ–secreting Th17 cells, with no significant impact on the amount of IL-17A$^+$ Th17 cells (Fig. 1, G and H). In contrast, CLF did not affect cytokine production from *C. rodentium*–elicited inflammatory Th17 cells (Fig. 1, G and H), which is consistent with the undisturbed clearance of *C. rodentium*. Therefore, inflammatory Th17 cells engaged in autoimmunity and infection are distinguishable populations with distinct responsiveness to CLF.

The distinction between proautoimmune and anti-infection Th17 cells is conserved across murine models

To address whether the distinction between autoimmune-derived and infection-elicited Th17 cells was caused by the absence of lymphocytes from *Rag1*$^{-/-}$ mice used in transfer colitis model, we tested the effect of CLF on Th17 cells from C57BL/6 mice in an anti-IL-10R–induced colitis model (Kullberg et al., 2006; Saha et al., 2021), an immune-mediated murine colitis model resembling human IBD. Mice receiving CLF showed less overall edema (Fig. 2, A and B) compared with vehicle control. Correspondingly, flow cytometry revealed a reduction in the frequency of IFN-γ–producing Th17 cells in the colon of CLF-treated mice relative to the vehicle control (Fig. 2, C and D; and Fig. S1 J), indicating a similar response as seen in the T cell transfer colitis in the *Rag1*$^{-/-}$ background.

On the other hand, a novel approach was designed to promote a *C. rodentium*–elicited Th17 response in *Rag1*$^{-/-}$ mice. Due to the importance of humoral immunity in *C. rodentium* control and clearance (Maaser et al., 2004), co-transfer of $CD19^+$ B cells and $CD25^-CD4^+$ T cells into a *Rag1*$^{-/-}$ host and infection with *C. rodentium* was conducted to determine the effect of CLF on the infection (Fig. 2 E). Both CLF and vehicle-treated mice survived the infection, but unexpectedly with stable colonization of *C. rodentium* (Fig. S1 K). Flow cytometry analysis at 3 wk after infection showed no significant difference in Th17 cell number or cytokine production between CLF and vehicle-treated mice (Fig. 2, F and G), which is consistent with the observations in C57BL/6 infection models (Fig. 1 G). These findings suggest the

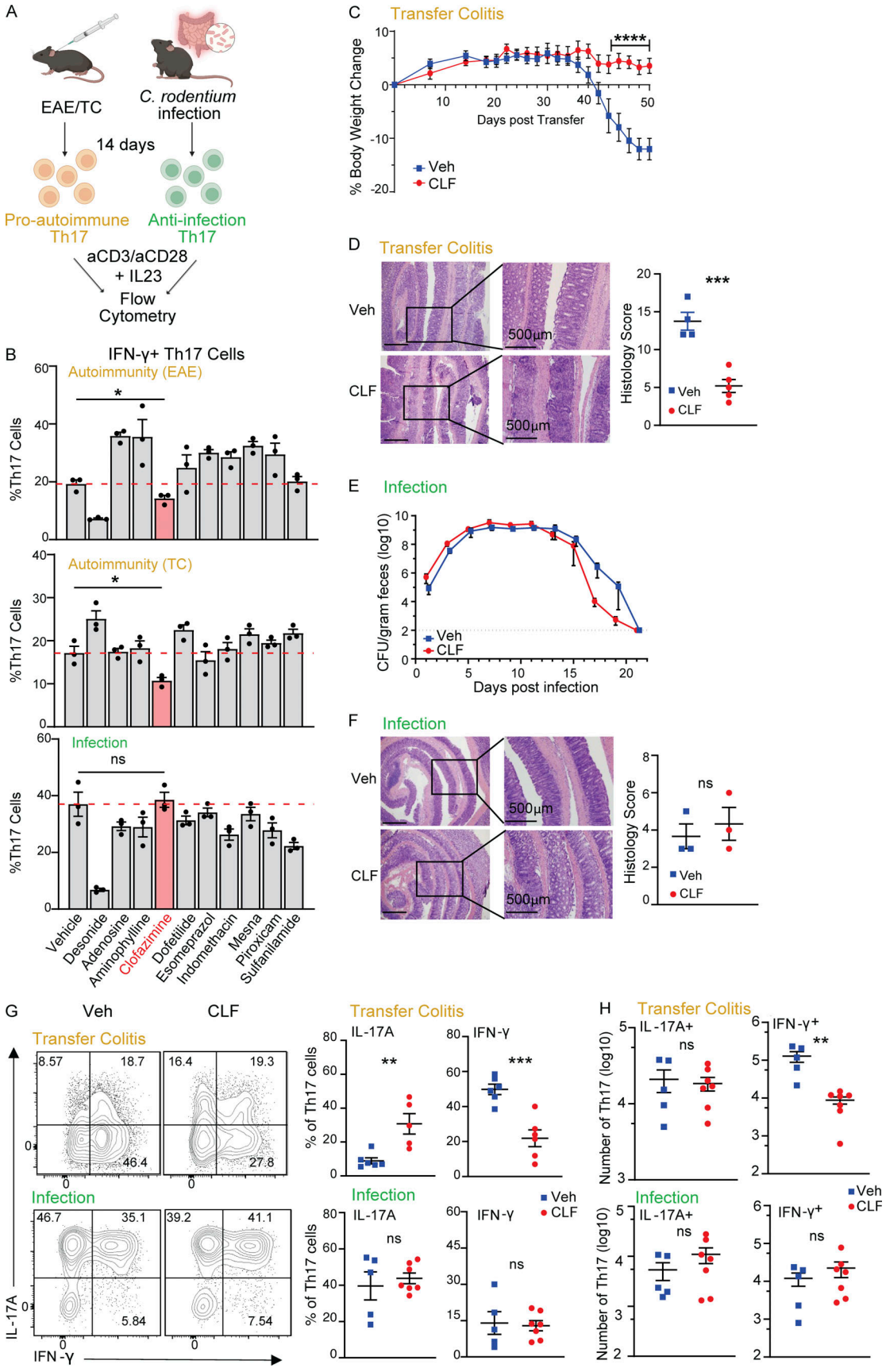

Figure 1. **Autoimmune-induced inflammatory Th17 cells are distinguishable from *C. rodentium*–elicited Th17 cells. (A)** Schematic diagram of ex vivo inflammatory Th17 stimulation. **(B)** Drug screen of ex vivo inflammatory Th17 cells. Quantification of IFN-γ⁺ Th17 cells using flow cytometry. Data

representative of two independent experiments. **(C)** *Rag1*$^{-/-}$ mice received naive T cells from WT donor and were treated intraperitoneally with CLF (n = 6) or vehicle (n = 6). Percent body weight change was shown relative to day 0. **(D)** Representative H&E staining of the colon of transfer colitis mice as shown in C at endpoint with histology scoring. **(E)** *C. rodentium* infection treated intraperitoneally with CLF (n = 7) or vehicle (n = 8). *C. rodentium* colonization curve determined by fecal shedding. **(F)** Representative H&E staining of the colon at peak infection of the mice as shown in E with histology scoring. **(G and H)** Flow cytometry of IL-17A$^+$ and IFN-γ$^+$ Th17 cells from the cLP of transfer colitis or *C. rodentium* infection treated with CLF reported in frequency (G) or absolute cell number (H). Statistical significance was determined using unpaired or multiple Student's t test. **(C–G)** Data are pooled and reported from two independent experiments. *, P < 0.05; **, P < 0.01; ***, P < 0.001; ****, P < 0.0001; ns, not significant; all data reported as mean ± SEM.

distinction between proautoimmune and anti-infection Th17 cells is conserved across different mouse model backgrounds. Thus, CLF selectively targets disease-promoting Th17 cells in both IL-10R–induced colitis and transfer colitis models.

Homeostatic Th17 cells are not disturbed by CLF treatment

As CLF is primarily used as an anti-leprosy drug, it is possible that it could affect the composition and localization of the microbiota. As such, we examined whether attenuated Th17-mediated autoimmunity following CLF treatment could be associated with altered microbiota. However, we found that the microbiota composition of healthy mice treated with or without CLF was similar, as demonstrated by α-diversity and Bray-Curtis principal coordinate analysis (PCoA; Fig. 2 H and Fig. S1 L). We observed only minor shifts in the *Firmacutes* and *Bacteroidetes* phyla after both treatment conditions (Fig. S1 M) with no significant changes overall.

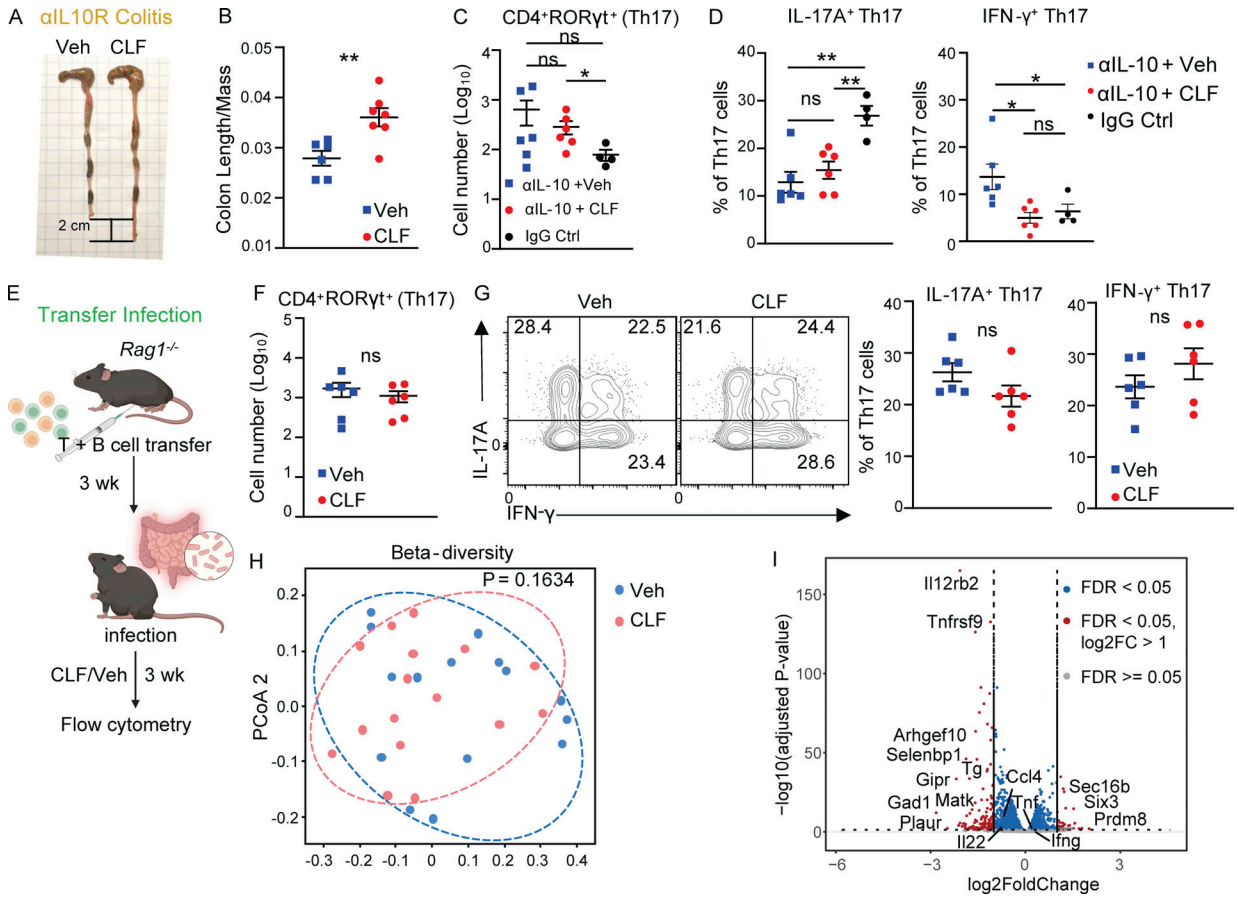

Figure 2. **The distinction between proautoimmune and anti-infection Th17 cells is conserved across murine models. (A–D)** WT mice were treated with CLF or vehicle after being given 0.5 mg/ml anti-IL10R antibody weekly for 4 wk. **(A)** Representative image of the colon from CLF- or vehicle-treated mice. **(B)** Length/mass ratio of the colons. **(C and D)** (C) Absolute number of Th17 cells or (D) frequency of IFN-γ$^+$ or IL-17A$^+$ Th17 cells from the lamina propria of anti-IL-10R–induced colitis treated with CLF or vehicle with IgG control mice. Data shown from two independent experiments. **(E–G)** Splenic naive CD4$^+$ T cells and CD19$^+$ B cells were sorted from WT donor and transferred into a *Rag1*$^{-/-}$ recipient at a 1:2 donor-to-recipient ratio. Recipients were infected 3 wk after cell transfer. **(E)** Schematic diagram showing the workflow of transfer infection model. **(F)** Absolute number of colonic Th17 cells. **(G)** Representative flow cytometry and frequency of IFN-γ$^+$ or IL-17A$^+$ Th17 cells. Data shown from two independent experiments. **(H)** Healthy WT mice were treated with CLF or vehicle control for 2 wk. Fecal shedding was collected pre- and post-treatment and analyzed using 16S rRNA sequencing. β-Diversity of the microbiota in CLF-treated mice was compared to vehicle control. Data shown from two independently housed groups from each treatment. **(I)** Bulk RNA-seq volcano plot of CLF treated in vitro differentiated homeostatic Th17 cells versus vehicle. Significant DEGs are determined by DESeq2 analysis and Benjamini-Hochberg adjusted P value. Statistical significance determined using unpaired or multiple Student's t test. *, P < 0.05; **, P < 0.01; ns, not significant; all data reported as mean ± SEM.

We also assessed the impact of CLF on homeostatic Th17 cells polarized in vitro and found that CLF did not affect gene expression profile, especially signature Th17 gene expression, of homeostatic Th17 cells, as demonstrated by RNA-sequencing (RNA-seq) analysis (Fig. 2 I). Therefore, we concluded that intestinal homeostasis and homeostatic Th17 cells are not disturbed by CLF.

Inflammation during *C. rodentium* infection and autoimmunity induce different inflammatory Th17 responses

To better understand the distinct responses of Th17 cells to CLF during inflammation, we performed single-cell RNA-seq (scRNA-seq) on colonic Th17 cells isolated from both *C. rodentium* infection and transfer colitis models at the peak of disease. *Rorc*$^{gfp/+}$ mice (Ivanov et al., 2006) were used in the infection model or as donor mice in the transfer colitis model, as their EGFP expression is controlled by RORγt (encoded by *Rorc*), allowing for viable isolation of Th17 cells (Fig. 3 A). We partitioned the 9,980 *Rorc*-expressing cells from the colon into five subsets, annotated as effector, proliferating, stem-like memory, myeloid-like, and epithelial-like subsets (Fig. 3 B).

The effector, proliferating, and stem-like memory subsets showed high expression of Th17 signatures. The effector cells had similar inflammatory transcripts to the proliferating cluster with lower expression levels, while stem-like memory cells exhibited exclusive expression of *Ccr7* and low expression of *Cd44* (Fig. 3 C and Fig. S2 A). Trajectory analysis revealed that effector Th17 cells transitioned toward clonal proliferation or stem-like memory cells (Fig. S2 B). We also identified a CD4$^+$ myeloid-like population expressing markers primarily restricted to the myeloid lineage (*Lyz2*, *Tgfbi*, *Il1a*, *Il1b*). Signature genes within these populations were highly comparable to those previously reported, confirming their T cell lineage despite lacking T cell markers (Kiner et al., 2021). Additionally, we found an epithelial-like population expressing antimicrobial genes and genes involved in mucosal barrier maintenance.

While the clusters were detected in both murine models (Fig. S2 C), the distribution patterns were significantly different (Fig. S2 D), indicating disparities among infection-elicited and proautoimmune Th17 cells. Furthermore, *Rorc*-expressing cells from CLF-treated transfer colitis mice revealed loss of key signature genes, including *Ifng*, *Il22*, and *Ccl4*, expression of which were all maintained during CLF treatment in Th17 cells from *C. rodentium* infection (Fig. 3 D). Thus, inflammatory Th17 cells in autoimmune colitis adopt a transcriptional program distinct from colonic infection–elicited Th17 cells.

We also investigated the effects of CLF on human Th17 cells engaged in IBD. Intestinal mononuclear cells were isolated from the colonic and ileal lesions of a patient diagnosed with Crohn's disease. After overnight CLF or DMSO treatment ex vivo, scRNA-seq analysis was performed on the gene expression profiles of 4,699 cells. About half of the total cells were clustered as T cells (Fig. S2, E and F). The CLF- and vehicle-treated groups showed similar cell clustering (Fig. S2 G), indicating that CLF treatment did not greatly impact any major populations. Consistent with published results, Th17 cells were distributed throughout the CD4$^+$ population, illustrating the heterogeneity and plasticity of Th17 cells adopting various inflammatory programs (Fig. S2 H). Some Th17 cells simultaneously co-expressed IL-17A and IFN-γ, while others only expressed IFN-γ, similar to Th1-like Th17 cells observed in mice (Fig. 3 E). CLF treatment repressed IFN-γ as well as multiple pathogenic gene expressions (Fig. 3 F), in line with the CLF's impact on proautoimmune Th17 cells in mice. These results suggest that the therapeutic effect of CLF in suppressing mouse Th17 pathogenicity may also be conserved in human Th17 cells in IBD.

Inflammatory Th17 cells in autoimmune colitis and infectious colitis are distinct in serine metabolism

scRNA-seq analysis on proautoimmune Th17 cells showed that CLF selectively targets important metabolic pathways such as one-carbon metabolism (Fig. S3 A). To understand the associations between metabolite levels and observed transcriptional changes, we investigated the metabolic phenotypes of proautoimmune Th17 cells. However, due to the small number of Th17 cells recovered from murine models, in vivo Th17 cell metabolomics was not feasible. Therefore, we used inflammatory Th17 cells polarized in vitro with IL-6, IL-1β, and IL-23 (IL23-Th17; Cua et al., 2003; Langrish et al., 2005; McGeachy et al., 2009). Although this differentiation scheme does not distinguish autoimmune and infection-elicited Th17 subsets, the polarized IL23-Th17 population represents proautoimmune Th17 cells as they can induce autoimmunity after adoptive transfer (Langrish et al., 2005). The vast majority of CLF-targeted genes in in vitro–polarized IL23-Th17 cells overlap with those in in vivo–committed proautoimmune Th17 (Fig. S3, B and C), indicating that IL23-Th17 reflects the characteristics of proautoimmune Th17 cells.

Metabolite set enrichment analysis revealed that treated Th17 cells have significantly increased intracellular serine (Fig. 4 A). To further confirm the elevation of intracellular serine levels by CLF in vivo, we FACS-sorted GFP$^+$ Th17 cells from both *C. rodentium* infection and transfer colitis models. In accordance with the observation from in vitro polarized cells, CLF enriched serine in vivo in proautoimmune Th17 cells whereas reduced this amino acid in infection-elicited Th17 cells (Fig. 4 B).

To understand the influence of serine accumulation on Th17 cell function, mice were fed with serine-supplemented drinking water (Fujita et al., 2016). Serine intake delayed the onset and progression of autoimmune colitis without affecting total number of Th17 cells (Fig. 4, C–E, and Fig. S3 D). However, serine reduced colonic IFN-γ$^+$ Th17 cells and increased IL-17A$^+$IFN-γ$^-$ Th17 cells—an effector state resembling that of CLF-treated Th17 cells (Fig. 4, C–F). In contrast, serine intake did not interfere with the clearance of *C. rodentium* (Fig. 4 D). Cytokine production from *C. rodentium*–elicited Th17 cells were comparable between mice fed water with and without serine (Fig. 4 F). Therefore, inflammatory Th17 cells in autoimmune colitis and colitogenic infection are distinctly dependent on serine metabolism, supporting the discrimination of proautoimmune and infection-elicited Th17 subsets.

Serine provides one-carbon units through mitochondrial folate pathway for the biosynthesis of purine as well as epigenetic methylation. Pathway analysis shows purine metabolism is enriched in CLF-treated IL23-Th17 cells (Fig. 4 G), leading us to

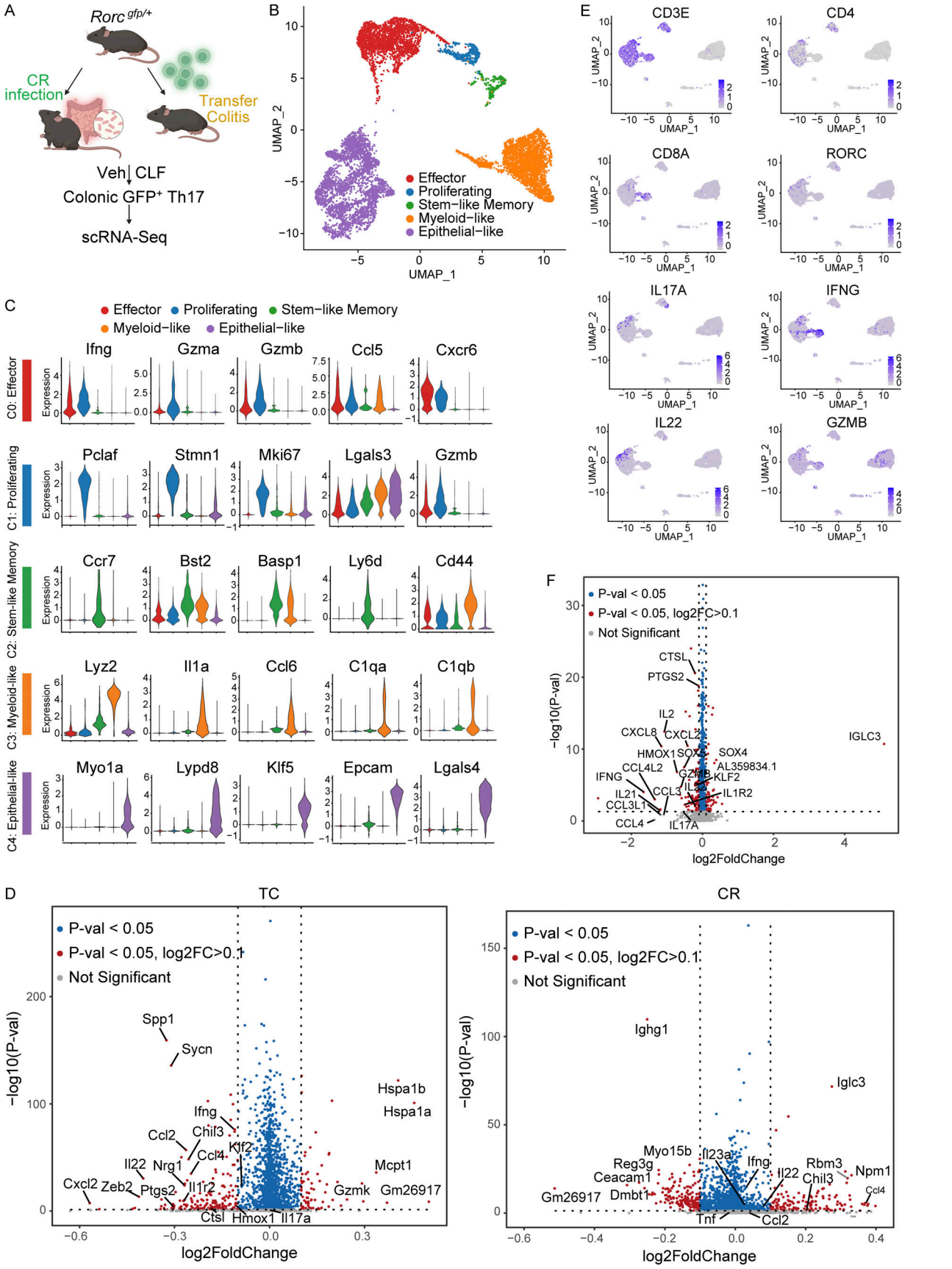

Figure 3. **Inflammation during autoimmunity and *C. rodentium* infection induce different inflammatory Th17 responses. (A)** *Rorc*$^{gfp/+}$ mice were used as donors for T cell transfer–induced colitis (TC) or infected with *C. rodentium* (CR). Schematic of FACS sorting of cells from the cLP used for scRNA-seq. **(B–D)**

scRNA-seq of FACS-sorted *Rorc-gfp*$^+$ cells (n = 5 for each model, pooled) from the cLP of each model treated with CLF or vehicle. **(B)** UMAP visualization of *Rorc-gfp*$^+$ cells. **(C)** Violin plots of signature genes contributing to cell annotation. **(D)** Volcano plots of DEGs from CLF treatment in transfer colitis (left) and *C. rodentium* infection (right). **(E and F)** scRNA-seq on mononuclear cells isolated from intestinal lesions of a IBD patient. The cells were treated with CLF or vehicle ex vivo. **(E)** UMAP expression patterns of indicated genes. **(F)** Volcano plots of DEGs in human Th17 cells from CLF treatment. Significant DEGs were determined by Bonferroni-adjusted P value (adj. P < 0.05) and $\log_2$-fold-change.

explore the epigenetic landscape of inflammatory Th17 cells in autoimmunity. Th17 cells were sorted from colitis mice transferred with naive *Rorc*$^{gfp/+}$ T cells for analysis of the global distribution of tri-methylated H3K4me3 (activator), H3K9me3, and H3K27me3 (repressor) detected by CUT&Tag, a highly sensitive alternative to chromatin immunoprecipitation sequencing. Next-generation sequencing revealed that H3K4me3 distribution was concentrated within the promoter regions while H3K9me3 and H3K27me3 were dispersed through intronic and intergenic regions of the genome (Fig. S3 E). Despite having little effect on H3K4me3 distribution, CLF treatment led to an increase in H3K27me3 at the promoter regions of proinflammatory cytokines, such as IFN-γ and IL-22, which was associated with their reduced expression in CLF-treated proautoimmune Th17 cells (Fig. 4, H and I). The increase in H3K27me3 levels was marginal for the promoter region of IL-17A (Fig. 4 J), indicating that H3K27me3 likely contributes to the selective repression of proautoimmune Th17 cells mediated by CLF.

Serine metabolic enzyme aldehyde dehydrogenase 1 family member 2 (ALDH1L2) is a CLF target selectively needed by inflammatory Th17 cell–mediated autoimmunity

To investigate the regulation of intracellular serine levels in proautoimmune Th17 cells, we profiled the transcripts of serine metabolic enzymes responsible for serine uptake (Kaplan et al., 2018), synthesis (Reid et al., 2018), and breakdown (Sugiura et al., 2022) in Th17 cells from vehicle- and CLF-treated autoimmune versus infectious colitis mice (Fig. 5, A and B). In proautoimmune Th17 cells, the top differentially expressed transcripts were ALDH1L1 and ALDH1L2, cytoplasmic and mitochondrial enzymes, respectively, responsible for converting one-carbon units derived from serine to CO_2, thereby shunting one-carbon units out of folate cycle (Krupenko et al., 2010; Fig. 5, A and B). However, none of these enzymes were targeted by CLF in infection-elicited Th17 cells (Fig. 5 B), whereas PHGDH, the rate-limiting enzyme for serine de novo synthesis, was repressed in these cells, consistent with the reduced intracellular serine levels observed in infection-elicited Th17 cells treated with CLF (Fig. 4 B). Thus, *Aldh1l1* and *Aldh1l2* are specifically targeted by CLF in proautoimmune Th17 cells.

The transcription level of *Aldh1l2* was dramatically upregulated in proautoimmune Th17 cells compared with infection-elicited cells (Fig. 5 C), leading us to explore the role of ALDH1L2 in proautoimmune Th17 cells. To this end, we transferred naive CD4$^+$ T cells from *Aldh1l2*$^{-/-}$ mice (Krupenko et al., 2020) to elicit autoimmune colitis in *Rag1*$^{-/-}$ recipient mice. The resulting *Aldh1l2*$^{-/-}$ CD4$^+$ T cells, enriched with Th17 cells, have significantly higher serine levels than their WT counterparts (Fig. 5 D). Conversely, the treatment of Th17 cells with serine did not affect the transcription of *Aldh1l2* (Fig. 5 E), indicating that ALDH1L2 plays a role in regulating intracellular serine levels in proautoimmune Th17 cells.

Consistent with CLF and serine treatment, *Aldh1l2*$^{-/-}$ T cell recipients exhibited attenuated transfer colitis and negligible weight loss (Fig. 5 F). Notably, loss of *Aldh1l2* abolished IFN-γ and IL-22 expression (Fig. 5 G) while conserving RORγt$^+$ cell number (Fig. S3 F). In contrast to previous conditions, loss of *Aldh1l2* resulted in only a minor decrease in IL-17A production, likely due to a mitochondrial or metabolic effect of the complete disruption of the folate cycle. The impact of *Aldh1l2* silencing was unique to proautoimmune Th17 cells since *C. rodentium*–elicited *Aldh1l2*$^{-/-}$ Th17 cells still controlled bacterial burden and cleared infection (Fig. 5 H). Isolated colonic Th17 cells had conserved cell number and cytokine production compared with WT cells, suggesting that *Aldh1l2* deficiency is not detrimental to inflammatory Th17 cells during infection (Fig. 5 I and Fig. S3 F). Furthermore, loss of *Aldh1l2* had no impact on in vitro polarization of suppressive regulatory T (Treg) cells (Fig. S3 G).

We confirmed the phenotype of *Aldh1l2*$^{-/-}$ mice by inducing autoimmune colitis through the depletion of IL-10R, which resulted in the observation that *Aldh1l2*$^{-/-}$ mice were more resistant to inflammation (Fig. 5 J) and Th1-like skewing of Th17 cells (Fig. 5 K). These findings indicate that proautoimmune and anti-infection Th17 cells have different dependencies on expression of the serine metabolic enzyme ALDH1L2. ALDH1L2 is necessary for the pathogenesis of autoimmunity and is targeted by CLF for selective suppression of proautoimmune Th17 cells.

We propose that CLF selectively targets proautoimmune Th17 cells partially by reducing *Aldh1l2* transcription, leading to an increase in intracellular serine and histone methylation. To confirm this mechanism of CLF function through ALDH1L2, we treated *Rag1*$^{-/-}$ mice that were adoptively transferred with naive *Aldh1l2*$^{-/-}$ CD4$^+$ T cells with CLF and tested for synergistic effects. As expected, we observed resistance to transfer colitis (Fig. 5 L and Fig. S3 H) with no synergistic impact on Th17 cytokine production relative to the *Aldh1l2*$^{-/-}$ vehicle control (Fig. 5 M). This observation suggests the important role of ALDH1L2 in mediating the effects of CLF on proautoimmune Th17 cells, further highlighting the importance of serine metabolism in distinguishing between autoimmune- versus infection-elicited Th17 cells.

Conclusions

Here, we present evidence that distinct environmental conditions in autoimmunity and infection result in the emergence of functionally distinct Th17 subsets, which can be distinguished based on their transcriptional and metabolic profiles. We demonstrate that CLF functions as a selective inhibitor of proautoimmune Th17 cells by increasing intracellular serine levels. Treatment with both CLF and serine significantly suppressed

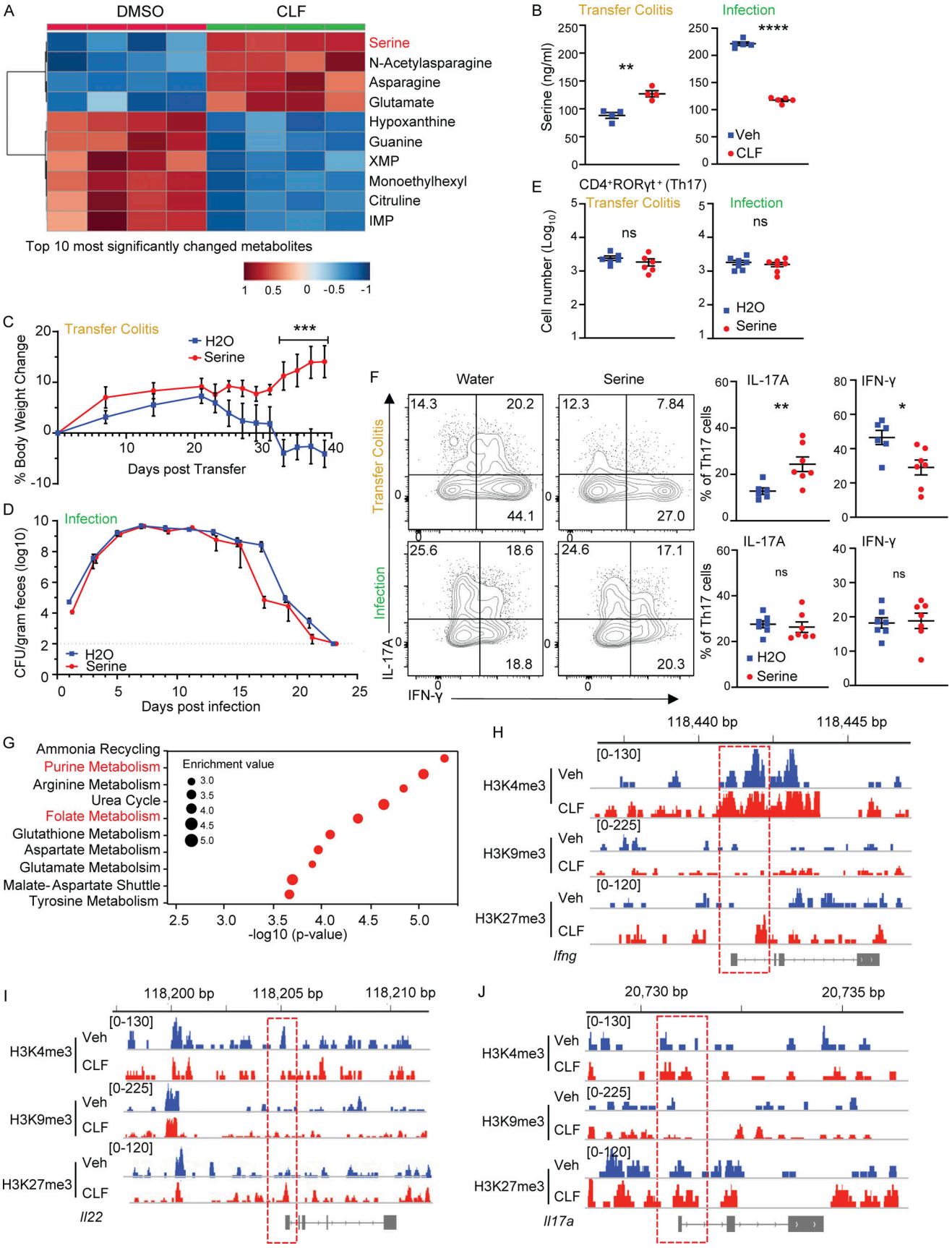

Figure 4. **Intracellular serine levels determine inflammatory potential of Th17 cells in autoimmunity. (A)** Targeted mass spectrometry of in vitro–differentiated IL23-Th17 cells treated with CLF or DMSO. Top differentially abundant metabolites in CLF-treated IL23-Th17 cells were listed. **(B)** Intracellular

serine levels of CD4⁺ cells from draining lymph nodes of mice with infection or transfer colitis treated with CLF or vehicle. **(C)** T cell transfer colitis recipients received serine-spiked (n = 7) or regular drinking water (n = 8) ad libitum. Body weight change of transfer colitis recipients was reported as percentage of starting body weight at day 0. **(D)** *C. rodentium*–infected mice received serine-spiked (n = 6) or regular (n = 7) drinking water ad libitum. *C. rodentium* colonization curve of the gut was determined from fecal shedding. **(E)** Absolute number of colonic Th17 cells. **(F)** Flow cytometry plots of IL-17A⁺ and IFN-γ⁺ cLP Th17 cells with quantified frequencies harvested at peak infection of *C. rodentium*–infected mice as shown in C or harvested at endpoint of T cell transfer colitis as shown in D. **(C–F)** Data shown from two independent experiments. **(G)** Metabolite set enrichment analysis of CLF-treated IL23-Th17 cell versus vehicle. **(H–J)** *Rorc-gfp*⁺ cLP cells were FACS-sorted from CLF-treated mice with transfer colitis–treated CUT&Tag sequencing peaks of H3K4, K9, and K27 trimethylation sites in sorted *Rorc-gfp*⁺ cells at promoter sites of signature Th17 gene, including *Ifng* (H), *Il22* (I), and *Il17a* (J). *, P < 0.05; **, P < 0.01; ***, P < 0.001; ****, P < 0.0001; ns, not significant. Statistical significance was determined by unpaired Student's t test. All data reported as mean ± SEM.

the Th1-like IFN-γ⁺ subset of Th17 cells in autoimmune colitis, while preserving IFN-γ secretion from Th17 cells during *C. rodentium* infection. Previous fate-mapping experiments of IL-17A–producing cells during EAE have shown that the majority of IFN-γ⁺ effector cells arise from IL-17A⁺IFN-γ⁻Th17 cell progeny (Hirota et al., 2011). Our findings suggest that different factors contribute to the formation of IFN-γ–producing Th1-like Th17 cells in autoimmunity versus infection, which likely accounts for the selective response of inflammatory Th17 cells to CLF and serine treatment. In addition, our data primarily reflect the responses of RORγt⁺ Th17 cells to CLF treatment. However, for Th1-like Th17 cells with diminished RORγt expression, it remains unclear if some cells completely cease expressing RORγt, which could potentially have been overlooked in our study.

Metabolic pathways such as glycolysis are essential regulators of Th17 inflammatory potential (Carriche et al., 2021; Wagner et al., 2021; Wang et al., 2015; Wu et al., 2020). However, targeting highly glycolytic Th17 cells in autoimmune diseases may not spare Th17 cells necessary for fighting against infections. Serine plays an essential role in T cell proliferation (Ma et al., 2017) by providing metabolic intermediates for nucleotide synthesis and methyl groups for biosynthetic and regulatory methylation reactions. Our data show that although CLF did not target the enzymes responsible for serine biosynthesis and uptake in proautoimmune Th17 cells, it significantly increased intracellular serine levels, indicating highly active serine catabolism in these cells prior to treatment. Several mitochondrial enzymes (MTHFD2, ALDH1L2) are crucial for serine breakdown, supported by our observation from *Aldh1l2*$^{-/-}$ mice and published data from *Mthfd2*$^{-/-}$ Th17 cells (Sugiura et al., 2022). Notably, proautoimmune Th17 cells have lower serine levels than infection-elicited population, reflecting a unique requirement for serine catabolites. Therefore, targeting Th17 cells dependent on serine catabolism might spare their counterparts elicited by infection.

Inflammatory Th17 cells have lower methylation levels than other T helper cells (Sugiura et al., 2022), perhaps due to the redirection of serine-derived methyl groups to polyamine synthesis (Carriche et al., 2021). Increases in intracellular serine from *Mthfd2*-deficient Th17 cells led to the elevation of histone methylation (H3K4me3 and H3K27me3; Sugiura et al., 2022). Although CLF's most significant effect on proautoimmune Th17 cells was an increase in serine levels, we did not observe increased H3K4me3. This finding could suggest that in vitro–differentiated Th17 cells may not adequately reflect the epigenetic state of intestinal Th17 cells.

In this study, we have uncovered a previously unknown immunoregulatory function of CLF, an FDA-approved leprosy drug (Garrelts, 1991), in selectively inhibiting proautoimmune Th17 cells by elevating intracellular serine. In a recent report, CLF inhibited potassium channels and thus repressed activation of Jurkat cells (Ren et al., 2008). However, the potassium channels of Jurkat cells are very different from those on primary T cells and other human T cell lines (e.g., CEM and MOLT-3; Feller et al., 2010), which might explain the different results between this study and ours.

Our data suggest that targeting Th17 cells dependent on serine catabolism might spare their counterparts elicited by infection, providing a potential avenue for precision therapy in autoimmune disorders. Notably, CLF was shown to selectively suppress proautoimmune Th17 cells while preserving inflammatory Th17 function during infection, which is a crucial need for autoimmune patients infected or exposed to pathogens. The distinguishable cell subsets with unique regulatory mechanisms identified in this study indicate that selective targeting of inflammatory Th17 cells in autoimmunity is feasible.

Although CLF has been used as an antibiotic in clinical trials for IBD (Afdhal et al., 1991; Prantera et al., 1994; Selby et al., 2007), our results suggest that its immuno-modulatory function may have been overlooked due to the presence of non-selective immunosuppressant steroids used in these trials. Furthermore, a combination therapy containing CLF and other broad-spectrum antibiotics has been patented for the treatment of multiple sclerosis (application #20140228307), but our findings demonstrate that CLF alone is sufficient to suppress EAE, supporting its antibiotic-independent potential as an immunomodulatory agent. However, the presence of long-lasting skin pigmentation, which represents an undesirable side effect of CLF, could potentially compromise its efficacy as a therapeutic option for autoimmune conditions.

In conclusion, this study provides insights into the mechanisms underlying Th17 cell regulation in autoimmune and infectious settings and highlights the feasibility of developing precise therapeutic interventions that selectively target disease-promoting Th17 for the treatment of autoimmune and inflammatory disorders without compromising infection clearance.

Materials and methods

Mice

All mice were obtained from The Jackson Laboratory, and select strains were bred in-house on a C57BL/6 WT background. Breeding for the strains C57BL/6, *Rag1*$^{-/-}$, *Rorc*$^{gfp/+}$, and *Aldh1l2*$^{-/-}$ were conducted in-house. All experiments were conducted

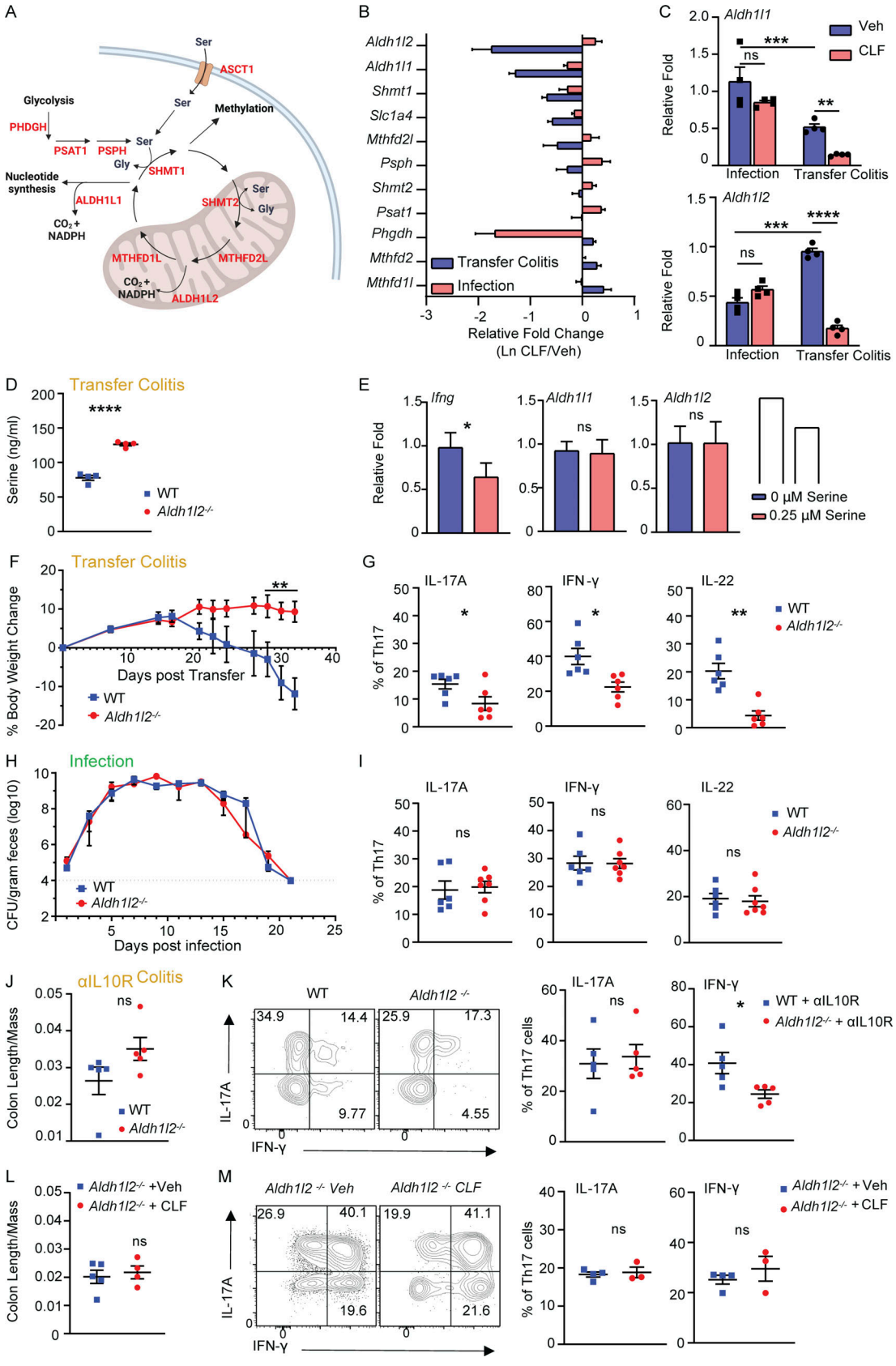

Figure 5. **ALDH1L2 is selectively needed by inflammatory Th17 cell–mediated autoimmunity. (A)** Metabolic pathway of serine and one-carbon metabolism. **(B)** Relative transcriptional fold change of key serine metabolic enzymes via real-time PCR on *Rorc-gfp*$^+$ cells sorted from cLP of CLF-treated mice during transfer colitis or *C. rodentium* infection. **(C)** Relative abundance of transcripts of *Aldh1l1* and *Aldh1l2* using *Rorc-gfp*$^+$ cells sorted from cLP of CLF-treated

mice during transfer colitis or *C. rodentium* infection. **(D)** Intracellular serine concentration from CD4+ T cells from the draining lymph nodes of *Aldh1l2*$^{-/-}$ mice with transfer colitis. **(E)** Relative abundance of transcripts of *Ifng*, *Aldh1l1*, and *Aldh1l2* in in vitro differentiated IL23-Th17 cells treated with and without serine. **(F and G)** WT or *Aldh1l2*$^{-/-}$ mice were used as T cell donors for transfer colitis. **(F)** Body weight change of transfer colitis recipients reported as percentage of starting body weight at day 0. **(G)** Frequencies of IL-17A+, IFN-γ+, or IL-22+ cLP Th17 cells using flow cytometry on cells harvested at endpoint. **(H and I)** WT or *Aldlh1l2*$^{-/-}$ mice were infected with *C. rodentium*. **(H)** Gut colonization curve determined from fecal shedding. **(I)** Frequencies of IL-17A+, IFN-γ+, or IL-22+ cLP Th17 cells using flow cytometry on cells harvested at peak infection. **(J and K)** WT or *Aldlh1l2*$^{-/-}$ mice were given 0.5 mg/ml anti-IL10R antibody weekly for 4 wk. **(J)** Length/mass ratio of the colons. **(K)** Representative flow cytometry (left) and frequencies (right) of IL-17A+ or IFN-γ+ cLP Th17 cells. Data representative of two independent experiments. **(L and M)** *Rag1*$^{-/-}$ mice were transferred with naive CD4+ T cells from *Aldh1l2*$^{-/-}$ mice, followed by vehicle or CLF treatment. **(L)** Length/mass ratio of the colons. **(M)** Representative flow cytometry (left) and frequencies (right) of IL-17A+ or IFN-γ+ cLP Th17 cells. Real-time PCR and differentiation data are from four technical replicates. Transfer colitis and infection data are each from two or more independent experiments. Statistical significance was determined by unpaired and multiple Student's *t* test. *, P < 0.05; **, P < 0.01; ***, P < 0.001; ****, P < 0.0001; ns, not significant. All data reported as mean ± SEM.

using mice 7–12 wk of age. Mice were housed in a specific-pathogen-free facility in Wake Forest School of Medicine Biotech Place Animal Facility. All protocols were approved by and in compliance with Wake Forest University's Animal Care and Use Committee. Mice were fed standard autoclaved chow and water and were kept on a 12-h light-dark cycle.

CLF treatment

CLF dosages were given at 25 mg/kg body weight and delivered in a corn oil solvent. Intraperitoneal delivery was conducted by injecting 100 µl of 4 mg/ml CLF or 100 µl corn oil as vehicle control every other day to achieve a human equivalent dose in clinical use (Nair and Jacob, 2016). In vitro CLF treatments were conducted at 1 µM for initial drug screen or 0.4 µM for all other in vitro experiments dissolved in DMSO. CLF treatment began on day 1 of *Citrobacter* infection model or day 14 of transfer colitis model and was continued every other day as described.

Ex vivo Th17 drug screen

For both stimulating conditions, WT mice were infected with *C. rodentium* as previously described (8–10 wk of age) or immunized subcutaneously with 200 µg $MOG_{(35-55)}$ emulsion and given 80 ng per mouse purified pertussis toxin (Hook laboratories) on day 0 and day 1 (10–12 wk of age) to induce EAE. Draining lymph nodes (mesenteric for infection, axillary for EAE, and inguinal lymph nodes for both) were harvested at day 14 after infection or immunization and homogenized through a 40 µm cell strainer to isolate T cells.

For αCD-3ε/αCD-28 Th17 activation, a 96-well flat-bottom tissue culture plate was coated with 1.5 µg Rabbit-αHamster IgG per well overnight at 4°C. The plate was washed with PBS, and 400,000 T cells per well were plated with 250 ng/ml αCD-3ε, 1 µg/ml αCD28, and 20 ng/ml IL-23 from each model. Cells were cultured in IMDM containing 10% FBS, presupplemented L-glutamine and Hepes, 50 µM β-mercaptoethanol, and antibiotics/antimycotics with 1 µg/ml of indicated drug. Cells were harvested at 48 h and stimulated with 20 ng/ml PMA, 1 µg/ml ionomycin, and 1× Golgi-stop for 4 h and stained and analyzed via flow cytometry (see Flow cytometry methods section). This experiment was performed and analyzed in triplicates.

Naive T cell sorting and transfer colitis induction

Splenocytes were harvested by passing a spleen through a 40 µm cell strainer from the indicated donor mouse (WT, *Aldh1l2*$^{-/-}$, or *Rorc*$^{gfp/+}$) at 8–10 wk of age. Naive CD4+ T cells were isolated using a negative magnetic bead selection and were stained for FACS sorting using antibodies in Table S1 for 20 min. Cells were washed and two-way sorted on a Beckman Coulter MoFlo Astrios EQ gating on the CD25−, CD4+, and CD45Rb^{hi} naive population using a 100 µm nozzle. Sort purity was checked by ensuring post-sorts were at least 85–90% pure. Cells were resuspended in PBS and transferred intraperitoneally to a *Rag1*$^{-/-}$ recipient (7–9 wk of age) at 400,000 cells/100 µl dose. Body weights and symptoms of colitis were monitored over the course of the model and humane endpoints varied within 4–6 wk after infection. CLF treatments began at day 14 (see CLF treatment) and serine-enriched water was provided ad libitum starting at day 0.

C. rodentium infection and shedding

C. rodentium was grown overnight at 37°C in LB broth agitated at 200 rpm. The approximate bacterial CFU concentration was determined from an OD_{600} standard curve. Both male and female mice ranging from 7 to 10 wk of age were used for infections. C57BL/6 and *Rag1*$^{-/-}$ mice were infected with ∼2.45 × 10^9 CFU of bacteria in 2% sucrose. Infection was given in two doses of 50 µl given 30 min apart. Bacterial loads were delivered orally by feeding the inoculum dropwise after 4–6 h of fasting. Actual CFU per dosage was determined by plating serial dilutions on MacConkey agar plates and incubating overnight at 37°C. *C. rodentium* gut colonization was followed by collecting fecal pellets to plate bacterial shedding. Fecal pellets were collected immediately after passing and were reconstituted in PBS at a 1:10 weight/volume dilution and homogenized on a Fisherbrand Bead Mill 24 at 2.1 speed for 1 min. Homogenates were pulse spun down to pellet debris and the supernatant was used for a serial 10-fold dilution to be plated onto MacConkey agar plates. After incubation overnight at 37°C, the gram-negative *C. rodentium* colonies can be identified as small pink colonies with a white edge and counted to back-calculate the CFU/gram feces. Shedding was monitored starting on day 1 after infection and was carried out every other day until clearance or humane endpoint was reached (20% body weight loss). Bacterial burden was cleared in ∼3 wk in WT mice and was fatal in *Rag1*$^{-/-}$ mice. CLF treatment began at day 1 and serine-enriched water was provided ad libitum at day 0.

Anti-IL-10r–induced colitis

C57BL/6 or *Aldh1l2*$^{-/-}$ mice were injected i.v. via tail vein with 0.5 mg/ml anti-mouse IL-10R IgG or anti-mouse IgG control

weekly over 4 wk for a total of 5 doses. WT mice were treated intraperitoneally with CLF or vehicle control starting on day 1 after i.v. Colon length and mass were weighed and disease severity was measured via flow cytometry of isolated colonic lamina propria (cLP) lymphocyte cytokine production.

Rag1$^{-/-}$ transfer *C. rodentium* infection model

From a WT donor spleen, CD19^{+} B cells were isolated using Miltenyi positive selection microbeads, and the flow through was used to isolate naive CD4^{+} T cells via StemCell Technologies mouse naive CD4^{+} negative selection kit. Cell fractions were pooled and transferred into *Rag1*$^{-/-}$ recipients intraperitoneally at a 1:2 donor to recipient ratio. 3 wk following transfer, mice were orally infected with *C. rodentium*, described above. Transfer infection mice were stably colonized by *C. rodentium* and cLP lymphocytes were isolated for flow cytometry at day 21 after infection.

T cell isolation from cLP

Cecum and colon were dissected from transfer colitis mice at endpoint and mice at peak *C. rodentium* infection. The large intestinal tract was cleared of fecal debris with PBS, flipped inside-out, cut into 1-cm pieces, and incubated in epithelial digest (RPMI containing 5% FBS, 5 mM EDTA, and 145 µg/ml dithiothreitol) at 37°C for 20 min shaking at 200 rpm. Tissue was vortexed, washed with PBS to remove EDTA and epithelia, and minced with scissors. Minced tissue was resuspended in enzyme digest (RPMI containing 5% FBS, 1 mg/ml collagenase D, and 100 µg/ml DNase) at 37°C for 40 min shaking at 200 rpm. Tissue was vortexed, pushed through a 70-µm cell strainer, and resuspended in 40% Percoll density gradient media. Cells were stacked onto 80% Percoll and spun at 500 × g for 25 min with no ramp or brake. Purified lymphocytes were harvested at interphase, washed, and prepared for downstream analysis.

Biopsy samples were obtained from human IBD patients with written informed consent. The study was approved by the Institutional Review Board, the Wake Forest School of Medicine, Winston Salem, NC, USA (protocol no. IRB00084249). Approximately 15 biopsy pinches from inflamed areas surrounding ileal and colonic lesions were collected from donors undergoing routine endoscopy procedure for Crohn's evaluation. Tissue pinches were digested in epithelial digest (RPMI containing 5% FBS, 1 mM EDTA, and 1 mM dithiothreitol) shaking at 37°C for 20 min. Tissue was vortexed, washed in PBS, and split into treatment conditions in enzyme digestion media (RPMI containing 10% FBS, 0.5 mg/ml collagenase VIII [Sigma-Aldrich], 0.6 mg/ml Dispase [Sigma-Aldrich], 100 µg/ml DNase) with 1 mM CLF or vehicle control. Tissues were incubated for 18 h overnight shaking 100 rpm at 37°C. Tissues were homogenized through 70-µm cell strainer, and lymphocytes were isolated through density gradient purification as described previously. Purified lymphocytes were stimulated with 5 nM PMA and 1 µg/ml ionomycin for 1 h followed by single-cell sorting and sequencing as described below for mouse Th17 cells.

Tissue preparation and H&E staining

The colon was isolated and cut open laterally to expose the intraepithelial membrane. It was washed vigorously with cold PBS to free fecal debris and mucous followed by a rinse with 10% buffered formalin. Colonic tissue was rolled on a pipette tip and transferred to a cassette which was stored overnight in 10% buffered formalin. Tissue was embedded in paraffin and slices of the entire length of the colon were placed on slides and stained with H&E stain. Representative micrographs of slides were captured on a Nikon Eclipse TE300 inverted microscope. Quantitative assessment of inflammation and tissue damage was completed by a trained pathologist (see Histology scoring).

Histology scoring

The scoring of H&E-stained slides was completed by a trained pathologist following eight criteria to assess tissue damage and inflammation. Scoring criteria are as follows: neutrophil infiltration (0: none, 1: 1–50 cells, 2: 50–100 cells, 3: >100 cells); edema (0: none, 1: mild, 2: moderate, 3: severe); goblet cell depletion (0: 50+/high-power field [HPF], 1: 25–50/HPF, 2: 10–25/HPF, 3: <10/HPF); crypt damage (0: intact, 1: basal 1/3, 2: basal 2/3, 3: entire loss); atrophy and crypt loss (0: normal crypt, 1: mild, 2: moderate, 3: severe); epithelial regeneration (0: complete, 1: slight injury, 2: surface not intact, 3: no tissue repair); epithelial hyperplasia (0: none, 1: 1–50%, 2: 51–100%, 3: >100%); and erosion and ulceration (0: none, 1: focal, lamina propria, 2: muscularis propria, 3: full thickness). Final quantitative score of acute inflammation and tissue damage was the totaled score of all criteria.

Microbiome analysis

Gut microbiome profiles were examined per our previously described methods (Clark et al., 2022; Nagpal et al., 2019; Rejeski et al., 2022; Saccon et al., 2021). Briefly, the Earth Microbiome Project benchmark protocol (http://www.earthmicrobiome.org) was employed by utilizing a barcoded high-throughput sequencing approach as described previously (Caporaso et al., 2012). Freshly collected fecal pellets from individual animals were stored at −80°C immediately after collection. Genomic DNA from 200 mg feces was obtained using the Qiagen PowerFecal Pro kit per the manufacturer's instructions. The 16S rRNA gene (V4 hypervariable region) was PCR-amplified (Walters et al., 2015); resulting amplicons were purified with AMPure XP kit; purified products were quantified using the Qubit-4 fluorimeter, and the amplicon library was generated as per the methods described previously (Caporaso et al., 2012). The purified PCR-amplicon product was pooled in equimolar concentrations and sequenced on an Illumina MiSeq sequencing platform using 2 × 300 bp sequencing kit (Miseq reagent kit v3). Automated cluster generation and paired-end sequencing with dual reads were performed as instructed by the manufacturer. The sequencing quality control was executed with on-board Miseq Control Software and Miseq Reporter. The .fastq files were processed with the QIIME2 (version 2.2021.2; https://qiime2.org/) bioinformatics pipeline (Bolyen et al., 2019) in a miniconda environment using the qiime2 EMPPairedEndSequences artifact (Clark et al., 2022; Nagpal et al., 2021; Saccon et al., 2021). The obtained sequences were demultiplexed based on unique barcodes assigned to each sample. Subsequent quality filtering, adapter trimming, denoising, and removal of non-chimeric amplicons

were carried out with the dada2 workflow by applying the qiime2-dada2 plugin using default parameters (Bokulich et al., 2018; Callahan et al., 2016). Alpha-rarefaction was performed at the lowest sequencing depth to avoid the bias of sequencing depth. Bacterial taxonomy was assigned to the amplicon sequence variants within qiime2 by implementing the Naive Bayes classifier (silva-138-99-515-806-nb-classifier.qza) natively implemented in dada2 and pretrained on SILVA reference database (version 138.1, updated March 2021) trimmed to the V4 domain (bound by the 515F/806R primer pair) with 99% sequence identity threshold, as described previously (Bokulich et al., 2018; Clark et al., 2022; Saccon et al., 2021). The dataset was filtered to omit features annotated as "mitochondria" and "chloroplast." Community richness (α-diversity) indices included Chao1 index and Shannon index. Community dissimilarities (β-diversity) were estimated by Bray-Curtis dissimilarity distance within qiime2. The resultant dataset was analyzed in two output forms: the raw abundance tables for amplicon sequence variants and their corresponding taxonomic assignments. The raw read counts were transformed to relative abundances by dividing each value by the total reads per sample and collapsed to taxonomic levels by summing their corresponding relative abundance. All samples were batch-processed to prevent any bias of variation due to DNA extraction, PCR primers/conditions, or sequencing library prepping protocols on microbial community composition obtained by amplicon sequencing.

All microbiome data were analyzed using the "R" statistical software package (version 4.1.2). The β-diversity was visualized by PCoA (principal coordinate analysis), and statistical analysis for differential clustering of samples on the PCoA plot was carried out by a permutational ANOVA test. α-Diversity was compared using two-tailed unpaired *t* test.

In vitro T cell differentiation

For T cell differentiation, 24-well tissue culture plates were coated with 200 ng/ml rabbit α-hamster IgG overnight at 4°C. Spleens were homogenized through a 40-µm cell strainer and resuspended in their appropriate differentiation conditions (homeostatic Th17—20 ng/ml IL-6, 2.5 ng/ml TGF-β; IL23-Th17—20 ng/ml IL-6, 20 ng/ml IL-23, 20 ng/ml IL-1β, 1 µg/ml αIFN-γ; Treg—2.5 ng/ml TGF-β with all conditions containing 250 ng/ml αCD-3ε and 1 µg/ml αCD-28) in IMDM containing 10% FBS, 50 µM β-mercaptoethanol, 1× antibiotics/antimycotics, presupplemented with L-glutamine and Hepes. Coating antibody was washed from a 24-well plate and cells were seeded at 400,000 (Th17) or 800,000 (Treg) cells per well in 2 ml of media. Cells were left to differentiate for 72 h (Th17) or 96 h (Treg) at 37°C until harvested for downstream analyses.

Th17 sorting and scRNA-seq

Colons of *Rorc*$^{gfp/+}$ recipient mice from transfer colitis or infected mice treated with CLF or vehicle were dissected and lymphocytes from the lamina propria were isolated (see T cell isolation from cLP). Cells were passed through an additional 40-µm cell strainer following density gradient. Cells were two-way sorted on a Beckman Coulter MoFlo Astrios EQ for GFP$^+$ cells on a 100 µm nozzle. Post-sorts were conducted to confirm a GFP$^+$ purity of 85–90%. Cells were sorted in media on ice until used for scRNA-seq. All scRNA-seq procedures were performed by the Cancer Genomics Shared Resource of the Wake Forest Baptist Medical Center Comprehensive Cancer Center. Viable cells (mean 83.4 ± 9.9%, n = 5) in suspensions averaging 995 ± 267 cell/µl were loaded into wells of a 10× Chromium single-cell capture chip targeting a cell recovery rate of 2,000–3,000 cells. Single-cell gel beads in emulsion were created on a Chromium Single Cell Controller and scRNA-seq libraries were prepared using the Chromium Single Cell 3′ Library and Gel Bead kit according to the manufacturers protocol (10 × Genomics). Sequencing libraries were loaded at 1.3 PM on an Illumina NextSeq500 with High Output 150 cycle kit (Illumina) for paired-end sequencing using the following read length: 26 bp Read1, 8 bp i7 Index, 0 bp i5 Index, and 98 bp Read2.

scRNA-seq data processing

The Cell Ranger Single Cell Software Suite v.2.0.1 was used to perform sample demultiplexing, alignment, filtering, and universal molecular identifier counting (https://support.10xgenomics.com/single-cell-gene-expression/software/pipelines/latest/what-is-cell-ranger). The data for each respective subpopulation were aggregated for direct comparison of single-cell transcriptomes. Low-quality cells were discarded if the cell number with expressed genes was smaller than 200. Cells were also removed if their proportions of mitochondrial gene expression were larger than 25%. Finally, a total of 9,980 single cells from T cell transfer–induced colitis and vehicle samples were captured.

Next, we used the Seurat toolkit (Stuart et al., 2019) to perform dimension reduction and cell clustering. Data were first loaded into R as a count matrix and log-transformed using the "NormalizeData" function. To remove batch effects, the count matrix from two samples was integrated using the "IntegrateData" function, resulting in a batch-corrected expression matrix. Subsequent principal component analysis was performed based on this batch-corrected data. After principal component analysis, the first 50 principal components are used for uniform manifold approximation and projection (UMAP) projection and cell clustering. Cells of the same type were clustered together in the UMAP. Cell annotations were then identified by the expressions of corresponding marker genes. Differentially expressed genes (DEGs) were identified using the "FindMarkers" function in the R package of "Seurat" (Butler et al., 2018). DEGs were evaluated with the Bonferroni-adjusted P value (adj. $P < 0.05$) and the $\log_2$-fold-change. Gene set enrichment analysis (Mootha et al., 2003; Subramanian et al., 2005) was used to interpret the enriched biological terms of DEGs.

Trajectory analysis

For trajectory analysis, we used the Monocle2 (Qiu et al., 2017) method to construct the single-cell trajectories of the Th17 population, including the effector, proliferating, and stem-like Th17 cells. "DDRTree" was applied to reduce dimensions and the visualization function "plot_cell_trajectory" was used to plot the minimum spanning tree on cells. Significance of DEGs was calculated with an approximate likelihood ratio test (Monocle2 differentialGeneTest() function) of the full model "~type" cells

against the reduced model "~1." 2,000 statistically significant genes with P < 0.005 and false discovery rate < 0.05 were used to construct the trajectory.

CUT&Tag assays

CUT&Tag (CUT&Tag-IT Kit from Active Motif) sequencing on histone trimethylation was conducted using *Rorc*$^{gfp/+}$ sorted cells from the cLP of transfer colitis mice (see Th17 sorting and scRNA-seq). Polyclonal rabbit antibodies for H3K4me3 (39159), H3K9me3 (39765), and H3K27me3 (39155) were used (all from active motif) to purify 300–500 bp chromatin fragments bound by trimethylated histones in duplicates. Sample libraries were multiplexed using Nextera i7 and i5 dual indices (Included in CUT&Tag-IT Kit from Active Motif) and sent for Illumina next-generation sequencing configured for 2 × 150 bp reads by Azenta Life Sciences. FASTQ files were uploaded to BasePair, aligned using Bowtie2 and CUT&Tag Peaks were called using MACS v2. Peak motifs were analyzed using HOMER. The recommended manufacturer's instructions were followed for all steps.

Metabolite profiling

Th17 cells were differentiated in vitro (see In vitro Th17 differentiation) with 0.5 µM CLF or DMSO added to differentiation media for 72 h. 5 million cells per sample were harvested for metabolomics analysis. For extraction of intracellular metabolites, cell pellets were resuspended in 1 ml of −80°C cold 80% MeOH, followed by incubation at −80°C for 20 min. Samples were pelleted at 4°C for 10 min at 15,000 rpm. The supernatants containing metabolites were harvested, while the cell pellets were re-extracted with 200 µl ice-cold 80% MeOH, spun down and the supernatants were combined. Metabolites were dried at room temperature under vacuum and resuspended in water for liquid chromatography–mass spectrometry analysis.

Samples were randomized and analyzed on a Q-Exactive Plus hybrid quadrupole-Orbitrap mass spectrometer coupled to Vanquish UHPLC system (Thermo Fisher Scientific). The mass spectrometer was run in polarity switching mode (+3.00 kV/−2.25 kV) with an m/z window ranging from 65 to 975. Mobile phase A was 5 mM NH_4AcO, pH 9.9, and mobile phase B was acetonitrile. Metabolites were separated on a Luna 3 µm NH_2 100 Å (150 × 2.0 mm) column (Phenomenex). The flow rate was 300 µl/min, and the gradient was from 15% A to 95% A in 18 min, followed by an isocratic step for 9 min and re-equilibration for 7 min. All samples were run in four biological repeats.

We detected 159 metabolites which were quantified as areas under the curve based on retention time and accurate mass (≤5 ppm) using the TraceFinder 4.1 (Thermo Fisher Scientific) software. The full panel of metabolites was then subjected to median normalization, cell number normalization, and finally z score normalization.

Flow cytometry and cytokine staining

In vitro or isolated primary cells were stimulated with 20 ng/ml PMA, 1 µg/ml ionomycin, and 10 mg/ml brefeldin A (GolgiStop, BD Biosciences) for 2 h at 37°C. Cells were stained with fixable viability stain (Zombie Aqua, BioLegend). Cells were stained for surface markers followed by intracellular cytokine staining using listed antibodies in Table S1 with eBioscience Foxp3/Transcription Factor Staining Buffer. Analysis by flow cytometry was conducted using a BD LSRFortessa X-20 cytometer and data were analyzed using FlowJo (v10.8.1). Th17 cells were defined and analyzed by gating on live, CD45$^+$, CD3ε$^+$, CD4$^+$, RORγt$^+$ cells.

Quantitative PCR (qPCR)

mRNA extracted from cells was used for cDNA synthesis via reverse transcriptase PCR, serving as template DNA in qPCR reactions. qPCR reactions were run using SYBR Green PCR Master Mix in an Applied Biosystems 7500 Real-Time PCR System using primers in Table S2. The ΔΔCt value was calculated and used to analyze relative gene transcript levels normalized to the β-actin control. All primers were run at optimal amplification efficiency with all measurements in duplicates run in two independent experiments.

Online supplemental material

Fig. S1 provides flow cytometry analysis of ex vivo screening assay and shows the effect of CLF on homeostatic and anti-infection Th17 cells. Fig. S2 contains supporting information for scRNA-seq analysis of mouse and human Th17 subsets. Fig. S3 includes the comparison between in vitro polarized Th17 cells and in vivo generated inflammatory Th17 cells as well as the impact of *Aldh1l2* deficiency on in vitro differentiation of Treg cells and disease severity of murine models. Table S1 contains the antibodies used for flow cytometry and sorting. Table S2 contains the primers used for real-time qPCR.

Data availability

The RNA-seq and scRNA-seq data are openly available in Gene Expression Omnibus (GEO) at GSE234594 (consisting of Sub-Series GSE234592 [scRNA-seq] and GSE234593 [RNA-seq]).

Acknowledgments

We thank J. Whitesides and J. Grayson (Wake Forest School of Medicine) for flow cytometry; W. Cui and Genomic Core staff (Wake Forest School of Medicine) for scRNA-seq. We thank I. Newman (UL1TR001420) for editing assistance.

S.A. Krupenko is supported by the National Institutes of Health (NIH) grant R01DK117854. J. Zhang is supported by NIH grant R00DE028973. Q. Song is supported in part by the Bioinformatics Shared Resources under the National Cancer Institute Cancer Center Support Grant to the Comprehensive Cancer Center of Wake Forest University Health Sciences (P30CA012197). Z. He is supported by the NIH grant UL1TR001420, R21AI166159 and R01AI173277, and Errett Fisher Foundation award. R.J. Bouch was supported by NIH grant 5T32A1007401-28.

Author contributions: R.J. Bouch designed, performed, and analyzed experiments and wrote the draft of the manuscript. J. Zhang, B.C. Miller, C.J. Robbins, and T.H. Mosher performed and analyzed experiments. R. Nagpal evaluated and interpreted microbiota data. W. Li evaluated and interpreted histopathology data. J. Zhao evaluated and interpreted metabolomics data. R.S. Bloomfeld collected human patient samples. Q. Song analyzed

and interpreted bioinformatic data. All authors contributed to writing the manuscript. Z. He conceptualized the study, interpreted the data, provided resources, secured funding, and edited and finalized the manuscript.

Disclosures: The authors declare no competing interests exist.

Submitted: 8 November 2022
Revised: 2 May 2023
Accepted: 14 June 2023

References

Afdhal, N.H., A. Long, J. Lennon, J. Crowe, and D.P. O'Donoghue. 1991. Controlled trial of antimycobacterial therapy in Crohn's disease. Clofazimine versus placebo. *Dig. Dis. Sci.* 36:449–453. https://doi.org/10.1007/BF01298873

Arbiser, J.L., and S.L. Moschella. 1995. Clofazimine: A review of its medical uses and mechanisms of action. *J. Am. Acad. Dermatol.* 32:241–247. https://doi.org/10.1016/0190-9622(95)90134-5

Awasthi, A., L. Riol-Blanco, A. Jäger, T. Korn, C. Pot, G. Galileos, E. Bettelli, V.K. Kuchroo, and M. Oukka. 2009. Cutting edge: IL-23 receptor gfp reporter mice reveal distinct populations of IL-17-producing cells. *J. Immunol.* 182:5904–5908. https://doi.org/10.4049/jimmunol.0900732

Bokulich, N.A., B.D. Kaehler, J.R. Rideout, M. Dillon, E. Bolyen, R. Knight, G.A. Huttley, and J. Gregory Caporaso. 2018. Optimizing taxonomic classification of marker-gene amplicon sequences with QIIME 2's q2-feature-classifier plugin. *Microbiome.* 6:90. https://doi.org/10.1186/s40168-018-0470-z

Bolyen, E., J.R. Rideout, M.R. Dillon, N.A. Bokulich, C.C. Abnet, G.A. Al-Ghalith, H. Alexander, E.J. Alm, M. Arumugam, F. Asnicar, et al. 2019. Reproducible, interactive, scalable and extensible microbiome data science using QIIME 2. *Nat. Biotechnol.* 37:852–857. https://doi.org/10.1038/s41587-019-0209-9

Butler, A., P. Hoffman, P. Smibert, E. Papalexi, and R. Satija. 2018. Integrating single-cell transcriptomic data across different conditions, technologies, and species. *Nat. Biotechnol.* 36:411–420. https://doi.org/10.1038/nbt.4096

Callahan, B.J., P.J. McMurdie, M.J. Rosen, A.W. Han, A.J. Johnson, and S.P. Holmes. 2016. DADA2: High-resolution sample inference from Illumina amplicon data. *Nat. Methods.* 13:581–583. https://doi.org/10.1038/nmeth.3869

Caporaso, J.G., C.L. Lauber, W.A. Walters, D. Berg-Lyons, J. Huntley, N. Fierer, S.M. Owens, J. Betley, L. Fraser, M. Bauer, et al. 2012. Ultra-high-throughput microbial community analysis on the Illumina HiSeq and MiSeq platforms. *ISME J.* 6:1621–1624. https://doi.org/10.1038/ismej.2012.8

Carriche, G.M., L. Almeida, P. Stüve, L. Velasquez, A. Dhillon-LaBrooy, U. Roy, M. Lindenberg, T. Strowig, C. Plaza-Sirvent, I. Schmitz, et al. 2021. Regulating T-cell differentiation through the polyamine spermidine. *J. Allergy Clin. Immunol.* 147:335–348.e11. https://doi.org/10.1016/j.jaci.2020.04.037

Clark, M., A.M. Centner, V. Ukhanov, R. Nagpal, and G. Salazar. 2022. Gallic acid ameliorates atherosclerosis and vascular senescence and remodels the microbiome in a sex-dependent manner in ApoE$^{-/-}$ mice. *J. Nutr. Biochem.* 110:109132. https://doi.org/10.1016/j.jnutbio.2022.109132

Collins, J.W., K.M. Keeney, V.F. Crepin, V.A. Rathinam, K.A. Fitzgerald, B.B. Finlay, and G. Frankel. 2014. Citrobacter rodentium: Infection, inflammation and the microbiota. *Nat. Rev. Microbiol.* 12:612–623. https://doi.org/10.1038/nrmicro3315

Cua, D.J., J. Sherlock, Y. Chen, C.A. Murphy, B. Joyce, B. Seymour, L. Lucian, W. To, S. Kwan, T. Churakova, et al. 2003. Interleukin-23 rather than interleukin-12 is the critical cytokine for autoimmune inflammation of the brain. *Nature.* 421:744–748. https://doi.org/10.1038/nature01355

Eden, K. 2019. Adoptive transfer colitis. *Methods Mol. Biol.* 1960:207–214. https://doi.org/10.1007/978-1-4939-9167-9_18

Feller, M., K. Huwiler, A. Schoepfer, A. Shang, H. Furrer, and M. Egger. 2010. Long-term antibiotic treatment for Crohn's disease: Systematic review and meta-analysis of placebo-controlled trials. *Clin. Infect. Dis.* 50:473–480. https://doi.org/10.1086/649923

Fujita, Y., T. Ishima, and K. Hashimoto. 2016. Supplementation with D-serine prevents the onset of cognitive deficits in adult offspring after maternal immune activation. *Sci. Rep.* 6:37261. https://doi.org/10.1038/srep37261

Garrelts, J.C. 1991. Clofazimine: A review of its use in leprosy and Mycobacterium avium complex infection. *DICP.* 25:525–531. https://doi.org/10.1177/106002809102500513

Gaublomme, J.T., N. Yosef, Y. Lee, R.S. Gertner, L.V. Yang, C. Wu, P.P. Pandolfi, T. Mak, R. Satija, A.K. Shalek, et al. 2015. Single-cell Genomics Unveils critical regulators of Th17 cell pathogenicity. *Cell.* 163:1400–1412. https://doi.org/10.1016/j.cell.2015.11.009

Ghoreschi, K., A. Laurence, X.P. Yang, C.M. Tato, M.J. McGeachy, J.E. Konkel, H.L. Ramos, L. Wei, T.S. Davidson, N. Bouladoux, et al. 2010. Generation of pathogenic T(H)17 cells in the absence of TGF-β signalling. *Nature.* 467:967–971. https://doi.org/10.1038/nature09447

Hirota, K., J.H. Duarte, M. Veldhoen, E. Hornsby, Y. Li, D.J. Cua, H. Ahlfors, C. Wilhelm, M. Tolaini, U. Menzel, et al. 2011. Fate mapping of IL-17-producing T cells in inflammatory responses. *Nat. Immunol.* 12:255–263. https://doi.org/10.1038/ni.1993

Hue, S., P. Ahern, S. Buonocore, M.C. Kullberg, D.J. Cua, B.S. McKenzie, F. Powrie, and K.J. Maloy. 2006. Interleukin-23 drives innate and T cell-mediated intestinal inflammation. *J. Exp. Med.* 203:2473–2483. https://doi.org/10.1084/jem.20061099

Ivanov, I.I., B.S. McKenzie, L. Zhou, C.E. Tadokoro, A. Lepelley, J.J. Lafaille, D.J. Cua, and D.R. Littman. 2006. The orphan nuclear receptor RORgammat directs the differentiation program of proinflammatory IL-17+ T helper cells. *Cell.* 126:1121–1133. https://doi.org/10.1016/j.cell.2006.07.035

Kaplan, E., S. Zubedat, I. Radzishevsky, A.C. Valenta, O. Rechnitz, H. Sason, C. Sajrawi, O. Bodner, K. Konno, K. Esaki, et al. 2018. ASCT1 (Slc1a4) transporter is a physiologic regulator of brain d-serine and neurodevelopment. *Proc. Natl. Acad. Sci. USA.* 115:9628–9633. https://doi.org/10.1073/pnas.1722677115

Kiner, E., E. Willie, B. Vijaykumar, K. Chowdhary, H. Schmutz, J. Chandler, A. Schnell, P.I. Thakore, G. LeGros, S. Mostafavi, et al. 2021. Gut CD4$^+$ T cell phenotypes are a continuum molded by microbes, not by T_H archetypes. *Nat. Immunol.* 22:216–228. https://doi.org/10.1038/s41590-020-00836-7

Krupenko, N.I., M.E. Dubard, K.C. Strickland, K.M. Moxley, N.V. Oleinik, and S.A. Krupenko. 2010. ALDH1L2 is the mitochondrial homolog of 10-formyltetrahydrofolate dehydrogenase. *J. Biol. Chem.* 285:23056–23063. https://doi.org/10.1074/jbc.M110.128843

Krupenko, N.I., J. Sharma, P. Pediaditakis, K.L. Helke, M.S. Hall, X. Du, S. Sumner, and S.A. Krupenko. 2020. Aldh1l2 knockout mouse metabolomics links the loss of the mitochondrial folate enzyme to deregulation of a lipid metabolism observed in rare human disorder. *Hum. Genomics.* 14:41. https://doi.org/10.1186/s40246-020-00291-3

Kullberg, M.C., D. Jankovic, C.G. Feng, S. Hue, P.L. Gorelick, B.S. McKenzie, D.J. Cua, F. Powrie, A.W. Cheever, K.J. Maloy, and A. Sher. 2006. IL-23 plays a key role in Helicobacter hepaticus-induced T cell-dependent colitis. *J. Exp. Med.* 203:2485–2494. https://doi.org/10.1084/jem.20061082

Langrish, C.L., Y. Chen, W.M. Blumenschein, J. Mattson, B. Basham, J.D. Sedgwick, T. McClanahan, R.A. Kastelein, and D.J. Cua. 2005. IL-23 drives a pathogenic T cell population that induces autoimmune inflammation. *J. Exp. Med.* 201:233–240. https://doi.org/10.1084/jem.20041257

Lee, J.Y., J.A. Hall, L. Kroehling, L. Wu, T. Najar, H.H. Nguyen, W.Y. Lin, S.T. Yeung, H.M. Silva, D. Li, et al. 2020. Serum amyloid A proteins induce pathogenic Th17 cells and promote inflammatory disease. *Cell.* 183:2036–2039. https://doi.org/10.1016/j.cell.2020.12.008

Ma, E.H., G. Bantug, T. Griss, S. Condotta, R.M. Johnson, B. Samborska, N. Mainolfi, V. Suri, H. Guak, M.L. Balmer, et al. 2017. Serine is an essential metabolite for effector T cell expansion. *Cell Metabol.* 25:345–357. https://doi.org/10.1016/j.cmet.2016.12.011

Maaser, C., M.P. Housley, M. Iimura, J.R. Smith, B.A. Vallance, B.B. Finlay, J.R. Schreiber, N.M. Varki, M.F. Kagnoff, and L. Eckmann. 2004. Clearance of Citrobacter rodentium requires B cells but not secretory immunoglobulin A (IgA) or IgM antibodies. *Infect. Immun.* 72:3315–3324. https://doi.org/10.1128/IAI.72.6.3315-3324.2004

McGeachy, M.J., Y. Chen, C.M. Tato, A. Laurence, B. Joyce-Shaikh, W.M. Blumenschein, T.K. McClanahan, J.J. O'Shea, and D.J. Cua. 2009. The interleukin 23 receptor is essential for the terminal differentiation of interleukin 17-producing effector T helper cells in vivo. *Nat. Immunol.* 10:314–324. https://doi.org/10.1038/ni.1698

Mootha, V.K., C.M. Lindgren, K.F. Eriksson, A. Subramanian, S. Sihag, J. Lehar, P. Puigserver, E. Carlsson, M. Ridderstråle, E. Laurila, et al. 2003. PGC-1alpha-responsive genes involved in oxidative phosphorylation are coordinately downregulated in human diabetes. *Nat. Genet.* 34:267–273. https://doi.org/10.1038/ng1180

Nagpal, R., N. Indugu, and P. Singh. 2021. Distinct gut microbiota signatures in mice treated with commonly used food preservatives. *Microorganisms*. 9:2311. https://doi.org/10.3390/microorganisms9112311

Nagpal, R., B.J. Neth, S. Wang, S. Craft, and H. Yadav. 2019. Modified Mediterranean-ketogenic diet modulates gut microbiome and short-chain fatty acids in association with Alzheimer's disease markers in subjects with mild cognitive impairment. *EBioMedicine*. 47:529–542. https://doi.org/10.1016/j.ebiom.2019.08.032

Nair, A.B., and S. Jacob. 2016. A simple practice guide for dose conversion between animals and human. *J. Basic Clin. Pharm.* 7:27–31. https://doi.org/10.4103/0976-0105.177703

Omenetti, S., C. Bussi, A. Metidji, A. Iseppon, S. Lee, M. Tolaini, Y. Li, G. Kelly, P. Chakravarty, S. Shoaie, et al. 2019. The intestine harbors functionally distinct homeostatic tissue-resident and inflammatory Th17 cells. *Immunity*. 51:77–89.e6. https://doi.org/10.1016/j.immuni.2019.05.004

Powrie, F., M.W. Leach, S. Mauze, S. Menon, L.B. Caddle, and R.L. Coffman. 1994. Inhibition of Th1 responses prevents inflammatory bowel disease in scid mice reconstituted with CD45RBhi CD4+ T cells. *Immunity*. 1: 553–562. https://doi.org/10.1016/1074-7613(94)90045-0

Prantera, C., A. Kohn, R. Mangiarotti, A. Andreoli, and C. Luzi. 1994. Anti-mycobacterial therapy in Crohn's disease: Results of a controlled, double-blind trial with a multiple antibiotic regimen. *Am. J. Gastroenterol.* 89: 513–518.

Qiu, X., Q. Mao, Y. Tang, L. Wang, R. Chawla, H.A. Pliner, and C. Trapnell. 2017. Reversed graph embedding resolves complex single-cell trajectories. *Nat. Methods*. 14:979–982. https://doi.org/10.1038/nmeth.4402

Reid, M.A., A.E. Allen, S. Liu, M.V. Liberti, P. Liu, X. Liu, Z. Dai, X. Gao, Q. Wang, Y. Liu, et al. 2018. Serine synthesis through PHGDH coordinates nucleotide levels by maintaining central carbon metabolism. *Nat. Commun.* 9:5442. https://doi.org/10.1038/s41467-018-07868-6

Rejeski, J.J., F.M. Wilson, R. Nagpal, H. Yadav, and R.B. Weinberg. 2022. The impact of a mediterranean diet on the gut microbiome in healthy human subjects: A pilot study. *Digestion*. 103:133–140. https://doi.org/10.1159/000519445

Ren, Y.R., F. Pan, S. Parvez, A. Fleig, C.R. Chong, J. Xu, Y. Dang, J. Zhang, H. Jiang, R. Penner, and J.O. Liu. 2008. Clofazimine inhibits human Kv1.3 potassium channel by perturbing calcium oscillation in T lymphocytes. *PLoS One*. 3:e4009. https://doi.org/10.1371/journal.pone.0004009

Ru, Y., X. Ding, Y. Luo, H. Li, X. Sun, M. Zhou, Y. Zhou, L. Kuai, M. Xing, L. Liu, et al. 2021. Adverse events associated with anti-IL-23 agents: Clinical evidence and possible mechanisms. *Front. Immunol.* 12:670398. https://doi.org/10.3389/fimmu.2021.670398

Saccon, T.D., R. Nagpal, H. Yadav, M.B. Cavalcante, A.D.C. Nunes, A. Schneider, A. Gesing, B. Hughes, M. Yousefzadeh, T. Tchkonia, et al. 2021. Senolytic combination of dasatinib and quercetin alleviates intestinal senescence and inflammation and modulates the gut microbiome in aged mice. *J. Gerontol. Biol. Med. Sci.* 76:1895–1905. https://doi.org/10.1093/gerona/glab002

Saha, P., R.M. Golonka, A.A. Abokor, B.S. Yeoh, and M. Vijay-Kumar. 2021. IL-10 receptor neutralization-induced colitis in mice: A comprehensive guide. *Curr. Protoc.* 1:e227. https://doi.org/10.1002/cpz1.227

Selby, W., P. Pavli, B. Crotty, T. Florin, G. Radford-Smith, P. Gibson, B. Mitchell, W. Connell, R. Read, M. Merrett, et al. 2007. Two-year combination antibiotic therapy with clarithromycin, rifabutin, and clofazimine for Crohn's disease. *Gastroenterology*. 132:2313–2319. https://doi.org/10.1053/j.gastro.2007.03.031

Shiomi, H., A. Masuda, S. Nishiumi, M. Nishida, T. Takagawa, Y. Shiomi, H. Kutsumi, R.S. Blumberg, T. Azuma, and M. Yoshida. 2010. Gamma interferon produced by antigen-specific CD4+ T cells regulates the mucosal immune responses to Citrobacter rodentium infection. *Infect. Immun.* 78:2653–2666. https://doi.org/10.1128/IAI.01343-09

Stuart, T., A. Butler, P. Hoffman, C. Hafemeister, E. Papalexi, W.M. Mauck, 3rd, Y. Hao, M. Stoeckius, P. Smibert, and R. Satija. 2019. Comprehensive integration of single-cell data. *Cell*. 177:1888–1902 e21. https://doi.org/10.1016/j.cell.2019.05.031

Subramanian, A., P. Tamayo, V.K. Mootha, S. Mukherjee, B.L. Ebert, M.A. Gillette, A. Paulovich, S.L. Pomeroy, T.R. Golub, E.S. Lander, and J.P. Mesirov. 2005. Gene set enrichment analysis: A knowledge-based approach for interpreting genome-wide expression profiles. *Proc. Natl. Acad. Sci. USA*. 102:15545–15550. https://doi.org/10.1073/pnas.0506580102

Sugiura, A., G. Andrejeva, K. Voss, D.R. Heintzman, X. Xu, M.Z. Madden, X. Ye, K.L. Beier, N.U. Chowdhury, M.M. Wolf, et al. 2022. MTHFD2 is a metabolic checkpoint controlling effector and regulatory T cell fate and function. *Immunity*. 55:65–81.e9. https://doi.org/10.1016/j.immuni.2021.10.011

Wagner, A., C. Wang, J. Fessler, D. DeTomaso, J. Avila-Pacheco, J. Kaminski, S. Zaghouani, E. Christian, P. Thakore, B. Schellhaass, et al. 2021. Metabolic modeling of single Th17 cells reveals regulators of autoimmunity. *Cell*. 184:4168–4185.e21. https://doi.org/10.1016/j.cell.2021.05.045

Walters, W., E.R. Hyde, D. Berg-Lyons, G. Ackermann, G. Humphrey, A. Parada, J.A. Gilbert, J.K. Jansson, J.G. Caporaso, J.A. Fuhrman, et al. 2015. Improved bacterial 16S rRNA gene (V4 and V4-5) and fungal internal transcribed spacer marker gene primers for microbial community surveys. *mSystems*. 1:e00009–e00015. https://doi.org/10.1128/mSystems.00009-15

Wang, C., N. Yosef, J. Gaublomme, C. Wu, Y. Lee, C.B. Clish, J. Kaminski, S. Xiao, G. Meyer Zu Horste, M. Pawlak, et al. 2015. CD5L/AIM regulates lipid biosynthesis and restrains Th17 cell pathogenicity. *Cell*. 163: 1413–1427. https://doi.org/10.1016/j.cell.2015.10.068

Withers, D.R., M.R. Hepworth, X. Wang, E.C. Mackley, E.E. Halford, E.E. Dutton, C.L. Marriott, V. Brucklacher-Waldert, M. Veldhoen, J. Kelsen, et al. 2016. Transient inhibition of ROR-γt therapeutically limits intestinal inflammation by reducing TH17 cells and preserving group 3 innate lymphoid cells. *Nat. Med.* 22:319–323. https://doi.org/10.1038/nm.4046

Wu, L., K.E.R. Hollinshead, Y. Hao, C. Au, L. Kroehling, C. Ng, W.Y. Lin, D. Li, H.M. Silva, J. Shin, et al. 2020. Niche-selective inhibition of pathogenic Th17 cells by targeting metabolic redundancy. *Cell*. 182:641–654.e20. https://doi.org/10.1016/j.cell.2020.06.014

Yen, D., J. Cheung, H. Scheerens, F. Poulet, T. McClanahan, B. McKenzie, M.A. Kleinschek, A. Owyang, J. Mattson, W. Blumenschein, et al. 2006. IL-23 is essential for T cell-mediated colitis and promotes inflammation via IL-17 and IL-6. *J. Clin. Invest.* 116:1310–1316. https://doi.org/10.1172/JCI21404

Yew, W.W., D. Liang, D.P. Chan, W. Shi, and Y. Zhang. 2017. Molecular mechanisms of clofazimine resistance in Mycobacterium tuberculosis. *J. Antimicrob. Chemother.* 72:2943–2944. https://doi.org/10.1093/jac/dkx227

JEM

Supplemental material

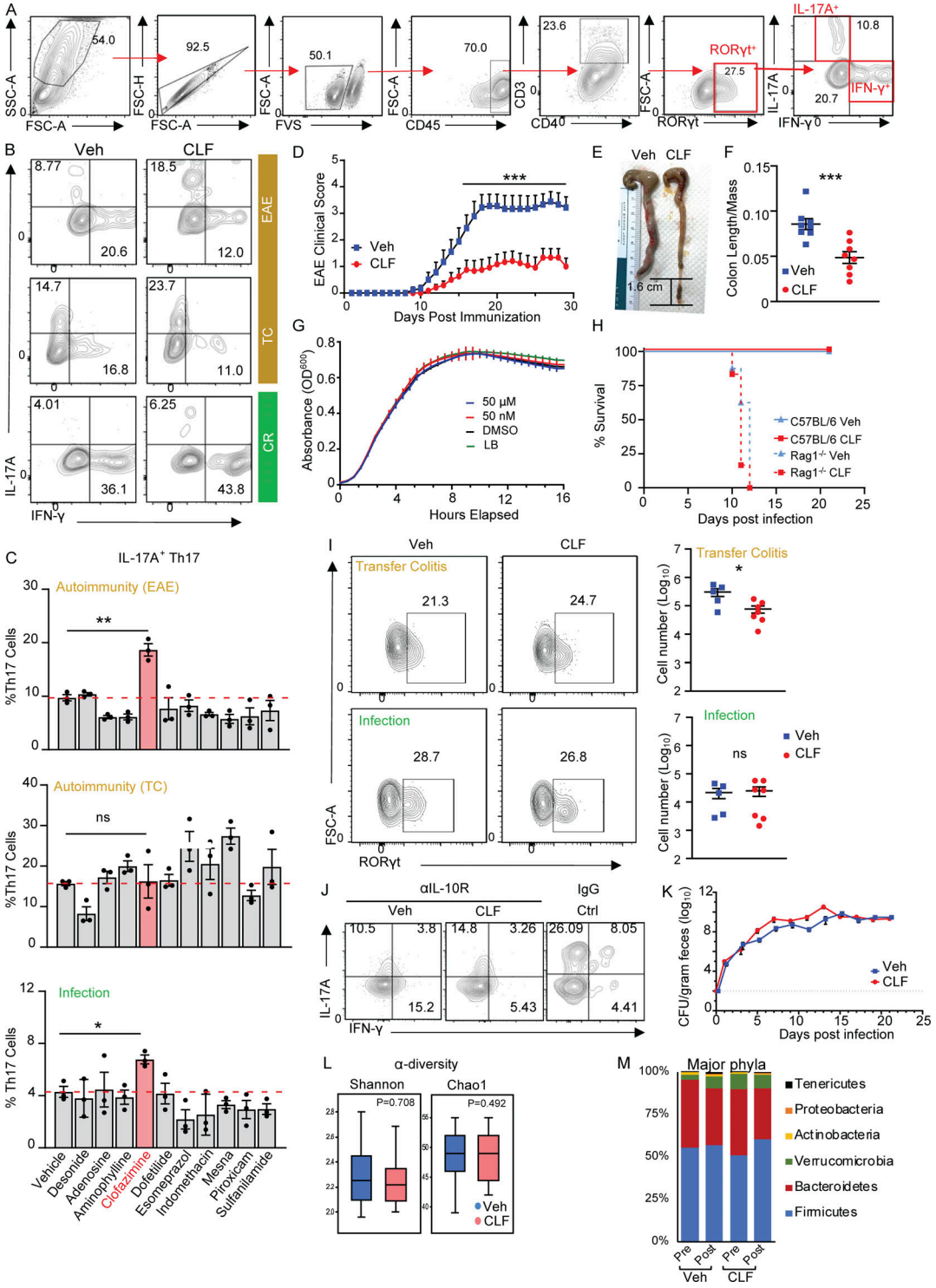

Figure S1. **CLF preserves homeostatic and infection-induced inflammatory Th17 cells. (A)** Flow cytometry gating strategy for drug-screen cytokine analysis. **(B and C)** Th17 cells isolated from indicated autoimmune or infection murine models were stimulated with αCD3ε/αCD28 and IL-23 for 48 h. **(B)** Representative flow cytometry dot plot. **(C)** Quantification of IL-17A$^+$ Th17 cells. **(D)** Clinical score of mice which were immunized with MOG_{35-55} to induce EAE and given CLF (n = 12) or vehicle (n = 9) every other day from day 1 after immunization. Data from two independent experiments. **(E and F)** Representative image (E) and length/mass ratio (F) of the colon from CLF- or vehicle-treated mice as shown in Fig. 1 C. **(G)** Growth curve of *C. rodentium* treated with CLF (n = 3 per group). **(H)** Kaplan-Meier survival curve of WT and *Rag1*$^{-/-}$ mice infected with *C. rodentium* and treated with CLF or vehicle (n = 5 per group). **(I)** Flow cytometry dot plot (left) and absolute number (right) of colonic Th17 cells from the models as shown in Fig. 1, C and D. **(J)** Representative flow cytometry plot of colonic Th17 cells from mice treated with anti-IL-10R as shown in Fig. 2 A. **(K)** *C. rodentium* colonization curve in *Rag1*$^{-/-}$ mice reconstituted with lymphocytes determined by fecal shedding. **(L)** α-Diversity. **(M)** and the composition of the microbiota in CLF-treated mice compared to vehicle control. *, P < 0.05; **, P<0.01; ***, P < 0.001; ns, not significant; Statistical significance was determined using unpaired Student's t test and (G) permutational ANOVA. All data reported as mean ± SEM. CR, *C. rodentium*. TC, transfer colitis.

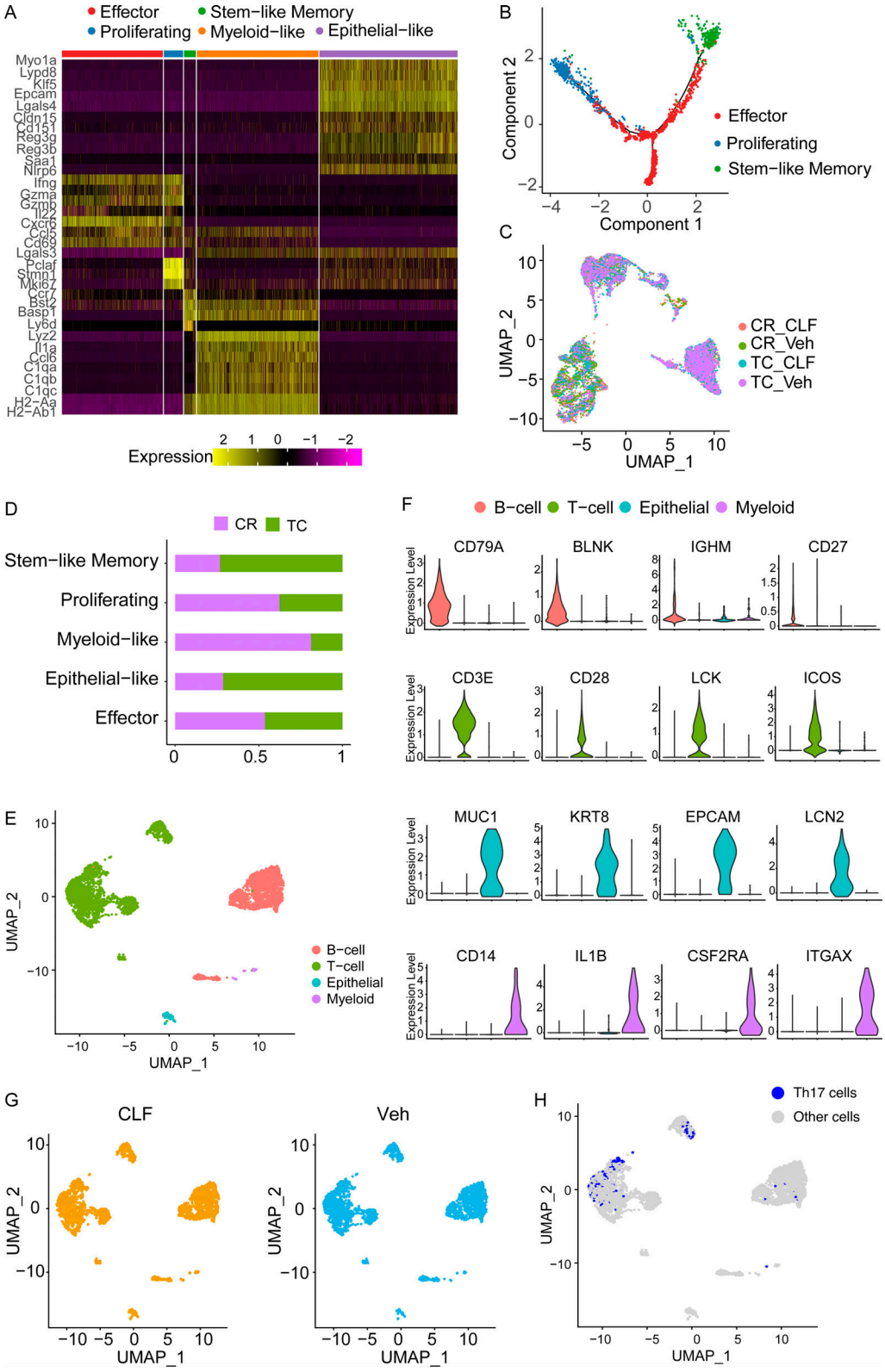

Figure S2. **Gene expression profile of mouse and human Th17 cells. (A–D)** *Rorc*$^{gfp/+}$ mice were infected with *C. rodentium* (CR) or used as donors for T cell transfer–induced colitis (TC). scRNA-seq of FACS sorted *Rorc-gfp*$^{+}$ cells from the cLP of each model treated with CLF or vehicle. **(A)** Heat map of signature genes contributing to cell annotation. **(B)** Trajectory analysis of effector, proliferating, and stem-like memory cluster. **(C)** Conditional UMAP showing distribution of each model and treatment. **(D)** Composition of each cluster from infection and transfer colitis model. **(E–G)** scRNA-seq was performed on mononuclear cells isolated from intestinal lesions of an IBD patient. The cells were treated with CLF or vehicle ex vivo. **(E and F)** (E) UMAP clustering of human IBD mononuclear cells and (F) violin plots of signature genes from each cluster. **(G)** Conditional UMAP showing distribution of each treatment. **(H)** UMAP expression plot of the distribution of *RORC*-expressing Th17 cells.

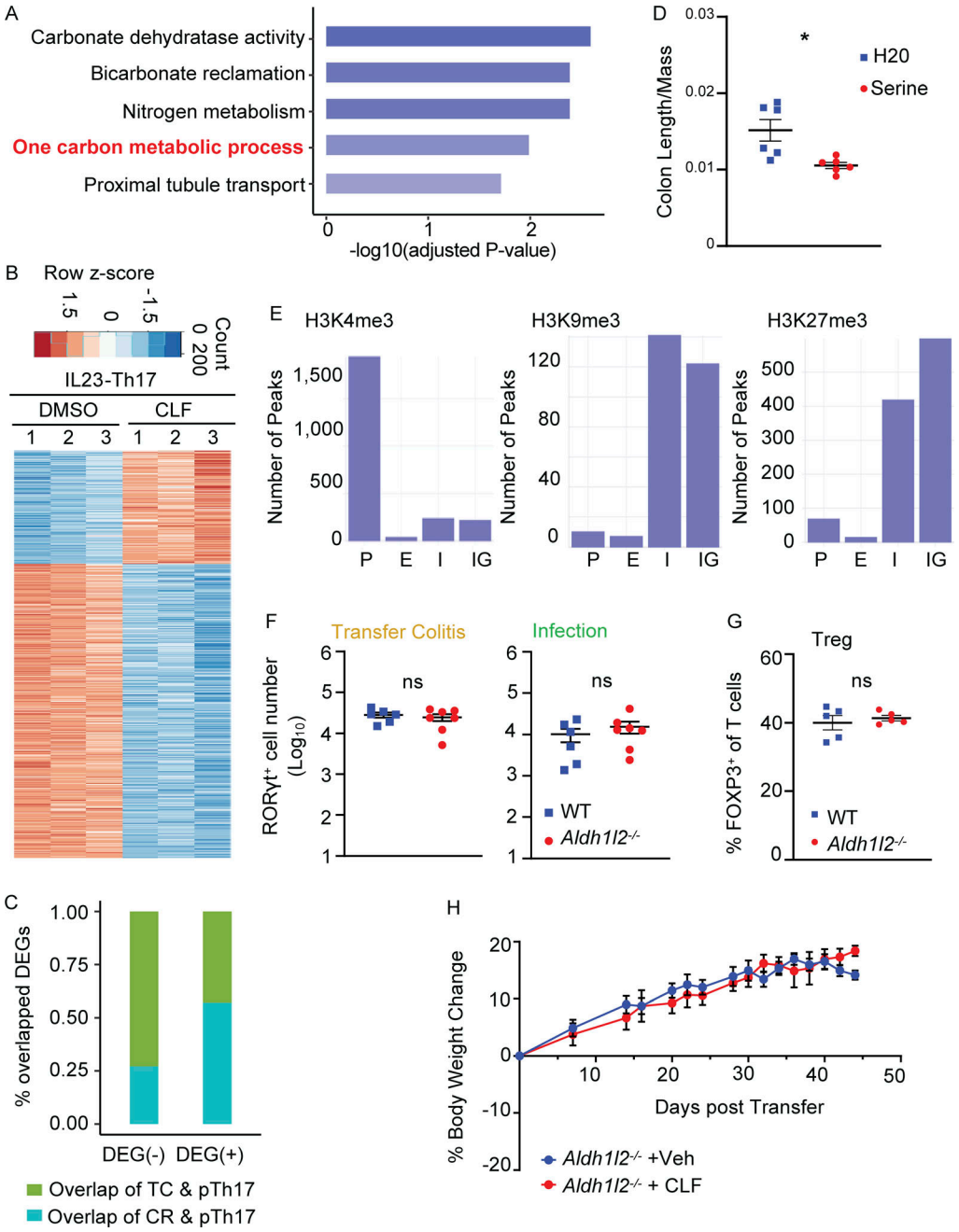

Figure S3. **CLF and exogenous serine inhibit in vitro differentiated pTh17 cells expressing a phenotype more like autoimmune inflammatory Th17 cells. (A)** Pathway enrichment analysis of DEGs identified by scRNA-seq of FACS-sorted *Rorc-gfp*$^+$ cells from the cLP of autoimmune colitis model treated with CLF or vehicle. **(B)** Global heat map of bulk RNA–sequenced in vitro–differentiated IL23-Th17 cells treated with CLF or DMSO. **(C)** Comparison of upregulated and downregulated DEGs between in vitro IL23-Th17 bulk RNA-seq (Fig. 4 A) and scRNA-seq from infection and autoimmune colitis model (Fig. 3). **(D)** Colon length/mass ratio from serine-treated mice with transfer colitis. **(E)** Distribution of H3K4, H3K9 and H3K27 tri-methylation peaks. **(F)** Absolute number of *Aldh1l2*$^{-/-}$ Th17 cells from cLP of mice with transfer colitis (TC) or *C. rodentium* (CR) infection as shown in Fig. 5, F–I. **(G)** Frequency of Treg cells from in vitro–differentiated *Aldh1l2*$^{-/-}$ naive T cells. **(H)** *Rag1*$^{-/-}$ mice were transferred with naive CD4$^+$ T cells from *Aldh1l2*$^{-/-}$ mice, followed by vehicle (n = 4) or CLF treatment (n = 4). Body weight change of transfer colitis recipients reported as percentage of starting body weight at day 0. P, promoter; E, exon; I, intron; IG, intergenic. *, P < 0.05; ns, not significant. Statistical significance determined using unpaired and multiple Student's t test. All data reported as mean ± SEM.

Provided online are two tables. Table S1 lists the antibodies for flow cytometry. Table S2 lists the real-time qPCR primers.